REMTECH Incorporated
2603 Artie Street, Suite 21
Huntsville, Alabama 35805

RTR 002-3

WING TIP VORTEX MEASUREMENTS WITH LASER DOPPLER SYSTEMS

April 1973

By

Charles E. Fuller, III

Prepared Under Contract NAS8-25896
for
Marshall Space Flight Center
Huntsville, Alabama

78

ABSTRACT

The vortex velocity field produced by a rectangular wing in a subsonic wind tunnel was measured using two laser Doppler Velocimeter systems. One system made three dimensional mean velocity measurements and the other made one dimensional turbulence measurements. The systems and test procedures are described and the measurements are presented and comparisons made. The data defined a strong spiral motion in the vortex formation process.

ACKNOWLEDGEMENTS

The studies described in this report were conducted under the technical direction of Mr. R. M. Huffaker of the Aero-Astrodynamics Laboratory of Marshall Space Flight Center, Huntsville, Alabama. Mr. Huffaker's guidance and encouragement were valuable throughout the the study.

The author wishes to express appreciation to Mr. Charles Craven of Lockheed Missiles and Space Co., Huntsville, Ala. for his co-operation and assistance in performing the experiments and analyzing the data.

The assistance of NASA/MSFC personnel, Mr. Arthur Hullett and Mr. Charles Albert in performing the experimental measurements is also gratefully acknowledged.

TABLE OF CONTENTS

1.0 INTRODUCTION

Recent measurements at Marshall Space Flight Center with a Laser Doppler Velocimeter (LDV) system have provided three dimensional velocity data in a wing tip vortex. These measurements were made to study vortex flow structure using a technique for obtaining three dimensional mean velocity data from the measurement of the Doppler frequency shift in laser light scattered by small particles in a gas flow. This technique used an LDV optical instrument designed to simultaneously collect forward scattered laser light from three different directions and to homodyne this light with reference laser light to produce a Doppler frequency output at three photo-detectors. The three Doppler frequencies were processed and stored in a signal analyzer where the mean Doppler frequency and its distribution were identified. With a knowledge of the geometry of the LDV instrument arrangement relative to the flow field and the measured Doppler frequencies, the three dimensional mean velocity vector of the particles causing the Doppler shift were computed. For very small particles the particle and fluid paths are approximately equal and the velocity measurement is considered to be that of the fluid.

This system has been used to make three dimensional mean velocity measurements in a vortex flow produced inside a subsonic wind tunnel by a rectangular wing at angle of attack. The optical, electrical and mechanical arrangements of this system are described and the equations relating the Doppler frequencies to the velocity components are presented and discussed. Typical displays of Doppler signals and three dimensional velocity profiles in the vortex region are presented.

In addition, one dimensional turbulence measurements were also made using a single component forward scatter LDV instrument and a frequency tracker. These measurements are also presented and described.

2.0 THE LDV SYSTEM

The LDV system is considered to be composed of all the equipment necessary for determining a gas velocity by measurement of the Doppler frequency shift in scattered laser light. This equipment includes an LDV instrument, an argon laser, and the electronic signal processing equipment.

The LDV instrument consists of two parts; a movable mount and an optical receiver. The movable mount supports the LDV instrument, laser and associated optics so that the components may be aligned and then moved in three orthogonal directions with a tolerance of $\pm$ 0.025 mm, thus allowing the measurements to be made at different points within a flow field.

The optical receiver houses the optical components necessary to collect three Doppler frequency shifted scatter beams and the reference or local oscillator (LO) beam. Physically the receiver consists of four metal tubes in which the optical components are rigidly held. Three of these tubes (scatter tubes) are arranged at 120° intervals around the fourth tube (LO tube) and collect the scatter light and direct it onto the photomultiplier detectors. The LO tube collects the reference beam, splits it into three segments and directs the segments to each of the three scatter tubes where homodyning with the scatter beam occurs. The physical design of the instrument allows for convenient positioning of the optical components through external adjustment.

Figure 1 shows a schematic of the optical arrangement of one of the scatter tubes and the reference beam tube. In this arrangement the laser beam

is focused at a known alignment point in the flow field to be measured. The alignment point is defined by the intersection of the laser beam and a small jet of air seeded with liquid silicon particles exhausting from a 0.50 mm diameter hollow needle.

The focal volume determined by the scatter tube optics is aligned so that it intersects with the focal volume of the reference beam at the alignment jet. The common volume formed by the intersection of these two beams is called the scattering volume. The scattering volume for the LDV system is the equivalent of the physical probe of convectional measurement systems, since this is the region in which the LDV data is taken. A variable front aperture and several interchangeable field stops are located in each scatter tube to allow for adjustment of the scatter volume size. The scatter volume is essentially an ellipsoid with a maximum length and width determined by the optical settings and angular arrangement of the instrument. As reported in Ref. 6, the width of the scatter volume was measured by moving a small alignment jet know distances along the width and observing the change in Doppler signal to noise (S/N) ratio. The width was found to be 0.10 mm. Using similar measurements made along the scatter volume length at scatter angles of 8.5° and 28° and reported in Ref. 6 and 7, Fig. 2 was prepared. This Figure shows the variation in scatter volume length with scatter angle for different ratios of S/N to maximum S/N in the length. Using this Figure the maximum scatter volume length for this test with a scatter angle of 12.6° was found to be 2.5mm.

From the alignment point, the reference beam passes into the reference tube where it is recollimated and directed onto a photomultiplier (RCA 8645).

An optical attenuator control provides a means for adjusting the reference beam power in order to obtain optimum Doppler S/N ratio. As shown in Ref. 1, coherent mixing theory requires that the reference power should be much greater than the scatter power in order to achieve optimum S/N. This should, however, be achieved without saturation of the photomultiplier tube as this can have adverse effects on the performance of the tube.

An acousto-optic-modulator is also included in the reference tube. A schematic of this device is given in Fig. 3. In this device a pizoelectric transducer is excited by a radio frequency (RF oscillator at either 19 or 57 MHz. The transducer then imports acoustic waves, at either of these frequencies in a glass block to which it is attached. The acoustic wave diffracts a fraction of the reference beam passing through it and shifts it in frequency by an amount equal to the acoustic or RF frequency, and in direction by an amount equal to twice the "Bragg" angle (arc sin $\lambda_{light}/2\ \lambda_{sound}$). As shown in Figure 3, an optical spatical filter consisting of a 2:1 magnification telescope and a 25 micron pinhole, isolates and collimates the frequency shifted laser beam, this beam being passed through the device and on to the photomultiplier tube to be used in homodyning with the light collected by the scatter tube. By homodyning this shifted light with the scatter light, the algebraic sign of the Doppler frequency shift can be determined and the direction of the calculated velocity vector, which would otherwise be ambiguous is fixed.

In each scatter tube, the first lens (L1 in Fig. 1) receives the scatter light at a distance of approximately 800 mm from the scatter volume and collimates it. The collimated light is then reflected off four mirrored

surfaces, in order to match the scatter beam and reference beam path lengths. The light is then focused by lens, L2, onto the field stop (FS1) which blocks light that does not originate within the focal volume. Following the field stop, lens L4 collects the light and focuses it onto the photomultiplier tube; passing first through a beam splitter which aligns it with the segment of reference light from the reference tube.

The necessity of equalizing the path lengths of the scatter and reference beams is a consequence of coherence length theory. The theory states that in order to maintain optimum homodyning the path length difference between the scatter and reference beams should be small in respect to the coherence length for the laser being used. This condition can be met by either increasing the laser coherence length with an etalon or by reducing the path length difference. In this instrument the path difference is minimized by movement of the outside mirrored prism until the maximum Doppler S/N is achieved.

In addition to the optical receiver and movable mount, the LDV system employs a CRL Model 53 continuous wave argon gas laser and the electronic equipment necessary for determining the mean Doppler frequency detected by the optical receiver. The argon laser is attached to the movable mount at a position opposite the optical receiver. A 2.5 watt output beam at 5145 Å is first passed through a beam expander and then onto a mirror. The mirror is attached to an adjustable mount which directs the beam through a focusing lens, through the flow field area and into the optical receiver. The adjustable mirror mount provides for the precise positioning needed for aligning the beam with the alignment jet and the reference tube of the optical receiver.

The final portion of the LDV system to be described will be that of

the electronic components used in determining the mean Doppler frequencies. For this discussion, the mean Doppler frequency refers to the frequency at which the Doppler signal distribution, as recorded and displayed by the electronics, was of maximum intensity. Figure 4 shows a schematic of the electronic signal processing equipment. In this arrangement the three Doppler frequencies from the photomultiplier (PM) tubes were amplified and initially processed and displayed by three spectrum analyzers. An improved S/N ratio displayed by the spectrum analyzers was provided by a signal analyzer (Hewlett-Packard Model 5480 with four channel plug-in) which processed the vertical output of each of the spectrum analyzers. The spectral display from each spectrum analyzer was stored in the signal analyzer as a series of 250 points in a magnetic core memory. The core storage could then be either displayed on a CRT or recorded with an X-Y plotter. In the Doppler measurements discussed here, each of the Doppler signals were in turn displayed on the CRT. The peak or maximum point of signal amplitude distribution was located and the frequency at that point identified by connecting a sweep oscillator to the spectrum analyzer input and adjusting the sweep oscillator frequency until it corresponded to the previously determined maximum point of Doppler frequency on the signal analyzer. The sweep oscillator frequency at that point was then read from a frequency counter.

The accuracy with which the mean Doppler signal could be detected was primarily dependent on the settings of the electronics and the distribution of the Doppler frequencies in the recorded signal. The most important electronic setting was the spectral width of the display. This importance can best be explained by the following example.

Consider that the spectral width on the spectrum analyzers were set at 1.0 MHz/cm. At this setting, the spectrum width on the signal analyzer CRT display would be 40 KHz/point, since there are 25 points/cm in the display. It is apparent that a position on the signal analyzer cannot be defined more accurately than one point, or in terms of frequency, more accurately than 40 KHz. Therefore, for a spectrum analyzer setting of 1.0 MHz/cm a frequency measured on the signal analyzer cannot be determined to within 40 KHz, and for wider or narrower spectrum analyzer setting the frequency identification accuracy will get correspondingly worse or better. How narrow the spectrum width can be set is determined by the spectral width of the Doppler signal. For the current measurements it was found that the best spectral width selection occurred when the Doppler signal occupied several centimeters of the CRT display. This usually occurred at 1 MHz/cm. The reasons for this consideration of frequency measurement accuracy becomes clearer when the LDV equations relating velocity to Doppler frequency are discussed in the following section.

Before concluding this section a brief discussion of several aspects of the particle-flow problem are considered. The fact that the LDV system measures particle velocities rather than fluid velocities immediately raises the question - "How well does the particle motion represent that of the fluid motion?". From the theoretical considerations reported in Ref. 2, it is noted that for particles with a size and density similar to that employed for the vortex tests, the difference between the particle and fluid velocities is expected to be less than 1%. In the remaining sections no distinction between particle and air velocity is made since the relative difference between the two is considered small.

Although for many applications, the particles which naturally occur in the air provide sufficient Doppler signals, such particles are usually in concentrations that do not provide a reasonably continuous scattering siganl (i.e. one particle per scattering volume). For the vortex measurements presented, particles of silicon liquid were seeded in the wind tunnel air supply. These particles were produced by passing compressed air out of small jets immersed in the liquid, causing the liquid to be sheared into small droplets forming an aerosol. Measurements of the particle size and concentration in the air supply showed particle concentrations of 2.08×10^6 particles/cm^3 with a mean particle size of 0.30 micron based on number. These measurements were made using a five stage casade impactor and the samples were taken from the air supply prior to tunnel operation.

In one region of the flow field, center of the vortex, the particle concentration was noticeably reduced. In that region the flow rotation is much the same as in solid body rotation. Particles are subjected to centrifugal forces which act to remove them from that region. This reduced the number of particles there and made the Doppler signals difficult to identify.

3.0 THREE DIMENSIONAL EQUATIONS

Although no rigorous derivation of the Doppler equations will be given here, an examination of the numerical values of the equations for particular geometrical arrangements are important in understanding the capabilities and limitations of a three dimensional measurement with this system.

Figure 5 shows a schematic of the geometric arrangement of the LDV optical receiver and reference beam relative to a flow field. In all applications considered to date, the angle Ψ, which is the angle between the reference

laser beam and the flow field axis, has been 90°. For Ψ=90° the defining set of equations are

$$\lambda F1 = (\sin\alpha)V + (\cos\alpha-1)W \quad (1)$$

$$\lambda F2 = (-3/2\ \sin\alpha)U - (1/2\ \sin\alpha)V + (\cos\alpha-1)W \quad (2)$$

$$\lambda F3 = (3/2\ \sin\alpha)U - (1/2\ \sin\alpha)V + (\cos\alpha-1)W \quad (3)$$

In the above equations λ is the laser wavelength (5145 A); α is the scattering angle; U, V, and W are the orthogonal components of mean velocity, and F1, F2, and F3 are the Doppler frequency components for each of the three scatter tubes. The LDV optical receiver is designed so that the scatter angle can be adjusted to nominal positions of 8°, 12°, 18°, and 28°. For the vortex test reported here the scatter angle on each tube was 12.6°.

In the following table the sensitivities of the Doppler frequencies to changes in the velocity components are tabulated for the 8.5°, 12.6°, 18°, and 28°.

Sensitivity	Scatter Angle			
MHz/m/sec	8.5°	12.6°	18°	28°
$\partial F1/\partial U$	0	0	0	0
$\partial F1/\partial V$	0.2878	0.4248	0.6003	0.9124
$\partial F1/\partial W$	-0.0213	-0.0469	-0.0948	-0.2273
$\partial F2/\partial U$	-0.2483	-0.3681	-0.5196	-0.7896
$\partial F2/\partial V$	-0.1433	-0.2122	-0.3001	-0.4560
$\partial F2/\partial W$	-0.0213	-0.0469	-0.0948	-0.2273
$\partial F3/\partial U$	0.2483	0.3681	0.5196	0.7896
$\partial F3/\partial V$	-0.1433	-0.2122	-0.3001	-0.4560
$\partial F3/\partial W$	-0.0213	-0.0469	-0.0948	-0.2273

It is instructive to note that the instrument arrangement is such that the sensitivity to changes in the W velocity component is much less than for the U and V components. From a practical measurement standpoint this means that

the Doppler frequency components must be identified with some precision in order for the W component to be meaningful. For example with a scatter angle of 12.6° (the case for the vortex measurements presented) a frequency error of $\pm$ 0.1 MHz in any Doppler frequency component would cause a W velocity error of $\pm$ 2.1 m/sec. Note that for a scatter angle increase to 28° a $\pm$ 0.1 MHz measurement error in any Doppler frequency component would only result in a W velocity error of $\pm$ 0.4 m/sec. It can then be clearly seen that a distinct advantage in sensitivity to the W velocity component is gained by increase in scatter angle. The W component sensitivity could likewise be improved by changes in the angle Ψ; however, such changes would present several mechanical and optical problems which would make the alignment and taking of data difficult, especially in a wind tunnel or other flow field which must be viewed through glass windows. For this reason the angle Ψ has always been made to be 90°.

As noted, the W sensitivity is improved by increasing scatter angle which is desirable when a three dimensional measurement is being made. There are several important consequences of this change which are worth mentioning. The increase in scatter angle will reduce the scatter volume size which is desirable if a high spatial resolution is to be achieved such as in flow fields with large velocity gradients. As a result of this decrease in scatter volume and an angular dependence of scatter intensity (the scatter intensity decreases with increasing angle from the reference beam), the amount of scatter power collected by the optical receiver will decrease resulting in a reduced Doppler signal level (assuming the reference laser beam power and scattering particle size and concentration are maintained). Increases in the

scatter angle will also cause the measured Doppler frequency shift to increase. In many applications it is possible to exceed the frequency response of the photo-detectors and/or other electronic measurement equipment when increasing the scatter angle. For example, if the velocity was 300m/sec in the U direction, then the Doppler frequency shift at 8.5° scatter angle on scatter tube 3 would be

$$F3=(\partial F3/\partial U)U = 0.248(300) = 74.5 \text{ MHz},$$

neglecting any contributions from the V and W directions. The corresponding Doppler frequency for a 28° scatter angle is 237 MHz, which is outside the range of the amplifiers presently used in the LDV system. Each test application must be examined to assure that an angular arrangement of the instrument can be provided which will produce the desired accuracy within the frequency and performance limitations of the system.

4.0 VORTEX MEASUREMENTS

Measurements were made using both the 3-Dimensional LDV system described in the previous sections and a one dimensional LDV instrument and frequency tracking system described in Ref. 3. The majority of the measurements were made with the 3-D system and were of the mean velocities in the vortex. The one dimensional system was used to obtain turbulence measurements.

The following sections present the results of these measurements.

4.1 THREE DIMENSIONAL DATA

Using the LDV system previously described, velocity measurements were made at the MSFC 7 x 7 inch wind tunnel facility. For these measurements a 6% thick biconvex constant cross-section wing with an aspect ratio of 2.7 was attached to the tunnel side wall at a +6° angle of attack. The wing had a chord of 6.57 cm (2.59 in.) and a semi-span of 8.89 cm (3.5 in.). The trailing edge of the wing was at the upstream edge of the side wall observation window and the wing extended to the middle of the tunnel. A schematic of the tunnel and LDV system arrangement is shown in Fig. 6.

The wing at angle of attack produced a wing tip vortex when the tunnel flow was initiated. This vortex flow, which trailed downstream of the wing, provided the velocity field in which the LDV measurements were made. The measurements were made at a station 1 and 2 span lengths (17.78 and 35.56 cm) behind the wing and with mean tunnel velocities of 80-84 m/sec as measured by a static pressure technique. Figure 6 also shows the wind tunnel coordinate system and directions for the measured velocity components. Table I gives the locations of the velocity profiles that were made. The majority of the

measurements were made at 2 span lengths from the wing.

Due to limited tunnel run time and limited data storage, only one data point per tunnel operation could be made. Although this limitation might be expected to cause some uncertainty in the reproducibility of the flow field for each point, the measurements show an exceptional degree of reproducibility with very little scatter in the data. Figures 7 through 33 present the velocity profiles for the U, V, and W velocity components in the vortex region. Several points can be made concerning the measurements. These are discussed under each of the velocity components.

For the U Velocity Component.

1. The profiles for the U component are presented in two forms. Fig. 10 through 15 show the velocity profiles in m/s while Fig. 16 through 21 show the same profiles non-dimensionalized by the total velocity V_T. The velocity profiles are presented in m/s to illustrate the slight variations in that component on either side of the vortex core. At about 9.4 cm from the tunnel sidewall a velocity deficite of about 1.5 m/s is noted in each of the profiles. This deficite is outside the wing tip and a corresponding deficite is not found on the inborad side of the vortex. The deficite is also noted at the one span location shown in Fig. 7, however, the deficite is only about 1.0 m/sec at this location. The oscillatory nature of these profiles are attributed to the roll-up or formation process of the vortex. It would be expected that the oscillations would disappear at stations further downstream and only the main velocity deficite associated with the vortex core would be present.

2. The measured profiles showed a
of 0.9 V_T ($V_T = (U^2 + V^2 + W^2)^{1/2}$) at one span downstream and 0
0.78 V_T at two spans downstream.

For the V Velocity Component

1. The maximum value of the V component was found to be 0.29 V_T at both the one and two span locations.
2. The diameter of the vortex core at the one span station was found to be 0.52 cm and 0.62 cm at the two span location. The core region is defined to be the region where the rotation is approximately equivalent to that of a solid body.
3. The V profile at the one span location indicated that the flow profile was not symmetric about the vortex core. In particular the profile has slightly higher velocities on the inboard side of the core than on the outboard side. The data at the 2 span location showed that the profile was much more symmetric, indicating that the vortex is more completely formed.
4. The profile at the one span location also showed a region on the outboard side of the core in which the velocity was almost constant for about 0.25 cm. This region corresponded to the region of the velocity deficite in the U component mentioned earlier. This flat region does not appear in the V profiles at the 2 span location, which would be expected since the region apparently corresponds to the deficite in the U component which was noted to be present at that station.

Identification of this region in the V profile probably would have been made if the data points had been more closely spaced.

5. The position of the vortex along the Y axis is determined by noting where the V component is zero. At the one span location the vortex is located at 0.5 cm inboard from the wing tip and at the two span location the vortex is located at 0.7 cm inboard from the wing.

For the W Velocity Component

1. Data at the one span measurement location (Fig. 9) shows that the W component changes direction at two positions along the Y axis. The outboard position for W = 0 corresponds to the position of the U velocity component deficite and the flat region in the V component profile previously mentioned. The fact that the W component remains negative as the measurements progressed inboard would indicate that this traverse is slightly below the center of the vortex core. The peak negative value corresponds to the position where the V velocity component (Fig. 8) goes to zero.
2. At the two span measurement location, Fig. 29 corresponds closely to Fig. 9 at the one span location. Both profiles indicate that they are below the vortex core. In addition, the profile in Fig. 33 would be above the vortex since this profile goes from negative to positive values in moving from the outboard to the inboard locations.

3. The fact that the W velocity component was found to be of the same order as the V component and in some cases higher, would indicate that the V component is not a good representation of the vortex tangential velocity. Assuming that the radial velocity component is small, the tangential velocity would be approximately equal to $\sqrt{V^2 + W^2}$ and if $V \approx W$ the peak tangential velocity would be higher than the V values by the $\sqrt{2}$. The assumption that the radial velocity component is small would probably only be good at points very close to the vortex core, since the flow further from that region is being pulled toward the core.

In observing the vortex measurements in perspective, the picture which evolves is one of a complex spiraling motion. It appears, that for the downstream stations at which the measurements were made, the vortex motion is not symmetric except at positions very close to the vortex core. Attempts were made at transforming the velocity data at the two span location into cylindrical coordinates. If any symmetry existed the data profiles could all be plotted on a single set of radial, tangential and axial curves. The results indicated that not such plots could be made.

Additional evidence of the lack of symmetric was obtained by photographing the vortex flow pattern. This was accomplished by passing a thin ($\approx$ 2mm) sheet of laser light through the wind tunnel flow and normal to the flow direction. The sheet of light was scattered by the silicon particles in the flow, thus allowing movie films to be made of the vortex flow patterns.

These films were taken through one of the wind tunnel windows. Figure 34 shows two of the enlarged frames from the movies. These frames further illustrate the spiraling nature of the flow. It is also interesting to note the reduced particle concentration in the core region. This reduced particle concentration caused some difficulty in obtaining data through that region. This is the reason no data was obtained in the core region on two of the profiles at the two span location.

4.2 DATA COMPARISONS

The wind tunnel vortex measurements conducted by Rorke and Moffitt and described in Ref. 4 provided data taken under measurement conditions that were very similar to those conducted by the author. For this reason their measurements were used for comparing with the author's data. Rorke's measurements were made with a triaxial hot wire probe with each element having a sensitive wire length of 1.25 mm and a diameter of 5 microns. The wing model was a NACA 0012 airfoil while that used by the author was a 6% thick biconvex airfoil. The perternate characteristics of comparison between the author's measurements and those of Rorke are given in Table II.

Figures 35 and 36 show comparisons of the author's profiles with those of Rorke for the conditions given in Table II. It is noted that Rorke's data shows only the axial and tangential velocities which were obtained from the U, V, and W velocity components assuming that the radial component was zero. The V velocity component of the author is used for comparison with Rorke's tangential velocity. Rorke's axial velocity would compare directly with the author's U velocity component. Several interesting points are noted and itemized below:

For Axial Velocity

1. The Author's axial velocity measurements exhibited profiles with several small dips as the core region was approached and a major dip which corresponded to the center of the vortex core, i.e. the largest dip occured at the points were the V velocity component was zero. This does not appear to be the case with Rorke's data, which shows that the major dip occurs at the position of maximum tangential velocity outboard of the wing. Rorke's data also shows much larger oscillations than that observed by the author.
2. Both sets of data show a larger decrease in the axial component in the vortex core as the distance from the trailing edge was increased. The maximum deficit noted by Rorke was 0.84 V_∞ and 0.78 V_∞ at the 2.0 and 5.0 chord locations while the author recorded maximum deficites of 0.9 V_∞ and 0.78 V_∞ at the 2.7 and 5.4 chord locations.
3. At the 5.0 chord location, Rorke also recorded a substantial reduction in the axial component both at inboard and outboard stations. This reduction was not evident in any of the author's data or in Rorke's data at the 2.0 chord station.

For Tangential Velocity

1. Generally Rorke's tangential velocity profiles show considerably larger peak vortex velocities than that recorded by the author's V component profile. As noted previously, the V component should be combined with the W velocity component to obtain the tangential velocity. This would have yielded peak tangential velocities that would have been

higher than that shown by the V component alone. The problem with that procedure is that the radial component must be assumed to be zero or small. The validity of such an assumption can be questioned on the grounds of the spiraling vortex motion that was observed.

2. The flat region in the profile observed by the author at the outboard station corresponded roughly with that observed by Rorke at the 2.0 and 2.7 chord stations. Rorke's data indicates that this flat region has grown into a dip at the 5.0 chord station. No dip was observed by the author at the 5.7 chord station.
3. In addition Rorke's data at the 5.0 chord station indicates that the tangential velocity has a direction reversal at about 2.0 cm from the core and inboard of the wing. The author's data did not indicate that this occured at the 5.7 chord station. There was also a substantially high tangential velocity in the outboard regions of the vortex core in Rorke's data which was not indicated in the Author's data.

The vortex core diameter, peak tangential velocity and mean axial velocity in the core have been found to be functions of the wing lift coefficient and the vortex age. For the wing used by the author the lift coefficient was calculated in the following manner from data in Ref. 5., pages 157-159. The lift coefficient is given by

$$C_L = a\,\alpha$$

where a is the slope of the lift curve slope and α is the angle of attack (6°). Also

$$a = a_0/(1 + a_0(57.3)/\pi e_1\,AR$$

Where a_0 is the slope of the lift curve for the section lift ($\approx .1082$ for the test airfoil), e_1 is the induced angle span efficiency factor and $e_1 = 1/1 + \tau = .8547$ for a rectangular wing span, and AR is the aspect ratio which is 2.75 for the test wing.

Using the above values

$$a = 0.571 \text{ and } C_L = .343$$

Also the vortex circulation strength is given by

$$\Gamma = C_L \; C \; V_T/2$$

Where C = chord length = 6.57 cm and V_T = total free stream velocity = 84 m/sec for this test.

Then

$$\Gamma = 0.970 \text{ m}^2/\text{s}$$

The vortex strength for the data of Rorke, with which the author's data was compared, had a value of

$$\Gamma = 1.36 \text{ m}^2/\text{s}$$

The vortex strength may also be estimated by assuming that the flow within the core region is circular and that the radial velocity component is zero. For this case the circulation strength is

$$\Gamma = 2\pi r \; V_{Tan} = \pi d V_{Tan}$$

Where d = core diameter and V_{Tan} = the tangential core velocity corresponding to that diameter. Using the above definition of vortex strength, calculations were made using the author's data and that of Rorke. This calculations are given in the following table.

Data	Chord Lengths from Wing	Core Dia. (cm)	V_{Tan} (m/s)	Γ (m^2/s)	t (millisec)
Rorke	2.0	.58	43.8	.797	4.0
Rorke	5.0	.78	43.2	1.058	8.6
Author	2.7	.42	25.0*	.324	2.6
Author	5.4	.65	25.0*	.510	5.2

* As noted previously the author's V velocity component which is used here is probably smaller than the actual tangential velocity.

An additional term of interest in vortex studies is that of vortex age. This term is defined as

$$t = \frac{d + .75c}{V_\infty}$$

Where V_∞ is the free stream velocity, d is the distance downstream from the wing trailing edge, and c is the wing chord length. In this expression, it is assumed that the vortex is formed at the quarter chord position. Values of the vortex age were calculated using the above definition and are shown in the preceding table.

Figure 37 shows a plot of the vortex strength as a function of vortex age for the tabulated data. The maximum vortex strength shown is taken to be the values calculated previously using the lift coefficient for the respective wings. This value represents the maximum vortex strength which can be achieved if all the wing vorticity is concentrated in the vortex. The data in Fig. 37 indicates that the vortex strength is still increasing at the vortex ages at which the measurements were taken. Thus, the vortex

is probably noted completely formed. Extentions of the data shows that the maximum vortex strengths are reached at a vortex age of 23-25 milliseconds. The trends in Fig. 37 are due to the increase in vortex diameter rather than an increase in vortex tangential velocity. As seen in the preceding table vortex tangential velocity was relatively constant between the two stations, while the diameter was still increasing. It would appear then that the maximum vortex tangential velocity is reached very quickly, and the vortex continues to increase its strength through a growth in core diameter.

This conclusion is contradicted by the data plotted in Fig. 38 which shows a plot of nondimensionalized core diameter as a function of vortex age. In the Fig. 38 the more extensive data of Rorke indicates that the maximum vortex diameter is reached in approximately 2 milliseconds. The Authors data, also shown, indicates that the diameter is still increasing at 5 milliseconds and as shown in Fig. 37 the maximum strength is not expected to be reached until 25 milliseconds.

The data comparisons show that there is a strong possibility that the maximum vortex strength was not reached in the author's measurements or those of Rorke. The increase in measured vortex strength appears to be caused by an increasing vortex core diameter with vortex age. This, however, is not substantiated by the more extensive data of Rorke, which shows that the maximum vortex diameter is reached quickly and begins to get smaller with increasing age. At some larger time the vortex diameter should begin to increase in size as the vortex dissipates.

Additional comparisons of the data were made with the theoretical developments of Hoffman and Joubert (Ref. 8) for turbulent line vortices. Their

formulation applies mixing length theory to concentrically circular turbulent flow, along with dimensional analysis considerations, to arrive at the conclusion that for values of $V_\infty X/\Gamma > 150$ the vortex flow field is independent of viscosity where V_∞ is the free stream velocity, X is the distance downstream and Γ is the vortex strength. They further conclude that if this condition is met a universal tangential velocity profile exists which can be written in terms of radial position at which the peak tangential velocity occurs. This relation is given as

$$V = \frac{V(max)\ r(max)}{r}\left[1 + 2.14 \log_{10} \frac{r}{r(max)}\right]$$

For values of r/r max < 0.4 V is defined by

$$V = \frac{1.83\ r^2}{r(max)}$$

Neglecting any spiral in the LDV data and assuming that the V velocity component represents the tangential velocity of a swirling symmetric vortex core, a comparison was made with a profile predicted by Hoffman and Joubert's equations. This is shown in Fig. 8. Their profile agrees well with the LDV data. It is noted that the agreement is better on the inboard portion of the wing with larger discrepancies observed on the outboard section. This discrepancy is attributed to the nonsymmetric nature of the profile which Hoffman and Joubert did not consider.

4.3 DOPPLER SPECTRAL DISTRIBUTIONS

Throughout the 3-D measurements the Doppler spectral distributions in the vortex region were of concern primarily because of a necessity of maintaining a good accuracy in the identification of the mean Doppler frequencies. The term mean Doppler frequency is taken to be the frequency at which the Doppler spectrum has a maximum signal intensity. This maximum point on the Doppler spectrum is the point at which the mean frequency has been identified for all the measurements presented.

Of particular interest is the F_1 frequency component. The F_1 frequency component has no sensitivity to the U velocity component, is most sensitive to the V component and approximately an order of magnitude less sensitive to the W component. The V velocity component will roughly correspond to the vortex tangential velocity for measurements made close to the vortex core. Since the tangential velocity distribution exhibits rather high velocity gradients and since the long dimension (0.5 mm) of the scatter volume is such that it sees this velocity spread, and further that the F_1 frequency component is most sensitive to this velocity, the broadening of the Doppler signal will be the greatest in the F_1 component for measurements close to and in the core. The spectrums of Fig. 39 do in fact show this to be the case. The signal in the top trace which is outside the core region is rather narrow and Gaussian in shape. The identification of the mean Doppler frequency at the peak intensity point is quite accurate for that measurement. Now note the changes in the signal trace as the core region is approached. The signal has definitely broadened to the point that a peak on the trace is rather hard to identify. The term mean Doppler frequency is much harder to define since the signal

strength is widely spread and not symmetrically distributed. Besides becoming broader the signal intensity is reduced due to the reduced particle concentrations.

Another characteristic of the F_1 Doppler spectrum is noted in the bottom trace of Fig. 39 . This trace shows a double hump in Doppler signal intensity. This type signal may be caused by a segregation of particles in the vortex region. The larger particles would tend to be located further from the vortex center with the smaller particles located closer to the center. The larger particles would produce a larger scatter of laser light and would therefore, be expected to produce a higher intensity Doppler signal. On the other hand, the smaller particles would produce less scatter and less Doppler signal per particle, however, the number of smaller particles could be expected to be greater than the large ones. It therefore, seems that such a particle segregation might cause the observed Doppler spectrum.

Since the nature of the Doppler spectrum near the core is rather broader and open to some amount of interpretation as to where the mean Doppler signal is located and also the core region is rather small, it was felt that the accuracy of the measurements could best be maintained by making measurements at a very close spacing. This spacing was 0.127 mm at points in the core region. Points at such a spacing allowed for a certain signal overlap since the scattering volume length was larger than this dimension. This signal overlap also helped to smooth any fluctuations or difference in the flow field from run to run, since only one point was made per operation of the wind tunnel.

So far in this discussion of Doppler spectral distributions no mention

has been made of the effects of turbulence on the observed signal broadening in the core region. An increase in turbulence intensity would definitely broaden the observed spectrum. The 1-D turbulence measurements did not conclusively indicate what effects the turbulence had on the broadening.

4.4 ONE DIMENSIONAL TURBULENCE DATA

The turbulence measurements were made using an LDV system and technique that was different from that used for the three dimensional mean velocity measurements. Only a brief description will be given here and the interested reader is directed to Ref. 3 for more complete details.

For the turbulence measurements, the wind tunnel coordinate system, wing configuration and operating conditions were the same as those used for the 3-D measurements. The LDV optical instrument was basically similar to the 3-D system in that the system operated on the reference -forward scatter technique. The instrument consisted of one component, i.e. scatter light was received from only one direction, thus only one velocity direction was obtained at a given time. The instrument was flexible in that measurements could be made from several different directions and at several different scatter angles. For the measurements made the system was placed in two different measurement configurations. One was to measure the V or tangential velocity along with the turbulence level, and the other configuration was to measure the U or axial velocity component.

A frequency tracker was used to obtain the turbulence data. This instrument was designed to accept the Doppler frequency as input data and to electronically "lock" onto the signal and track the frequency changes. The tracker

outputs are a DC voltage corresponding to the mean Doppler frequency or flow velocity and a fluctuating voltage level (AC) corresponding to the Doppler FM fluctuations or flow turbulence. With the use of calibration curves, the Doppler input frequencies can be identified and the corresponding mean velocity and turbulence levels are calculated using techniques described in Ref. 6.

Figure 40, 41, and 42 presents the mean velocity as well as the turbulent intensity distributions for the measurements made with the one dimensional instrument. Several operational difficulties limited the data taking capability. One of these was the short run time associated with the wind tunnel. During a run only about 30 sec was available for locking onto the Doppler signal and obtaining an accurate readout of the AC and DC output voltages. Another difficulty was encountered in the lower limit at which the frequency tracker would operate. This limit was 5 MHz which corresponded to a mean velocity of 12.5 m/sec. As shown in Fig. 41 the tangential velocity component was only above 12.5 m/sec in a very small region around the vortex core. One final operational difficulty was the reduced signal level which occured in the vortex core. The reduced signal level was a result of the reduced particle concentration in the core caused by the vortex motion which removed larger particles from the core. With the reduced signal level, the trackers would not maintain lock and no turbulence data could be obtained.

In Fig. 40 the axial velocity data is presented. The mean velocity profile shows the expected "dip" at the vortex core, while the local turbulence intensity is found to be approximately constant at about 5% and showing increases to 10% close to the core.

The tangential velocity component distribution given in Fig. 41, shows the expected shape and agrees well with profiles measured with the 3-D system. Figure 42 shows the local turbulent intensity distribution for the tangential velocity measurements. This data shows a large scatter and it is difficult to decern any trends. The measurements indicate a local turbulence intensity level of approximately 15% close to the core.

5.0 CONCLUSIONS AND RECOMMENDATIONS

Based on the results of the vortex measurements conducted, the following conclusions are drawn:

1. The techniques for routinely obtaining 3-dimensional mean velocity measurements and 1-dimensional turbulence using the laser Doppler technique was established.
2. The increase in vortex core size rather than an increase in the maximum core tangential velocity appears to be the governing parameter in the build-up of vortex strength. This conclusion is not supported by the data of Rorke (Ref. 4).
3. The vortex had not built up to its maximum strength at two span lengths from the trailing edge.
4. The turbulent intensity in the axial direction increases in the vortex core, and in the tangential direction the local turbulent intensity is about 15%.
5. The signal broadening resulting from the large velocity gradients in the core region made the determination of the maximum Doppler

frequency more difficult, but did not appear to increase the measurement error.

6. The vortex in the regions investigated is in a definite spiral motion in which the radial velocity component should not be neglected. Only these regions very close to the core are symmetric.
7. Oscillations in the axial (U) velocity component appear to be associated with the vortex formation process and correspond to similar perturbations in the other velocity components.
8. The non-uniform distribution of signal intensity in the vortex region indicates that the flow field has created regions in which the particles are not uniformly distributed, i.e. the particles appear to have been segregated according to size.

The following recommendations are set forth:

1. Use the 3-D system along with the three available frequency tracking systems to conduct further, more extensive studies of the vortex formation for various wing tip configurations.
2. Conduct further investigations into the probable segregation of particles in the vortex flow to determine if the technique might be used to measure particle sizes and concentrations.

6.0 REFERENCES

1. Rolfe, E. et. al., "Laser Doppler Velocity Instrument," NASA CR-1199, December 1967.

2. Huffaker, R. M., Fuller, C. E. and Lawrence, T. R., "Application of Laser Doppler Velocity Instrumentation to the Measurement of Jet Turbulence," Rept. 690266, Jan. 1969, International Automotive Eng. Congress, Detroit, Mich.

3. Fridman, J. E. and Meister, K., "Wide Band Frequency Tracker Performance," Final Report, NAS8-21293, December 1970, Raytheon Co.

4. Rorke, J. B. and Moffitt, R. C., "Wind Tunnel Simulation of Full Scale Vorticies," NASA CR-2180, March 1973.

5. Dommasch, D. O. et. al. Airplane Aerodynamics, Pitman Publishing Corp., New York, 1961.

6. Fuller, C. E., "Three Dimensional Laser Doppler Velocimeter Turbulence Measurements in a Pipe Flow," RTR-002-2, Final Rept. NAS8-25896, REMTECH Inc., Huntsville, Ala., April 1973.

7. Fuller, C. E., "Development Testing and Application of a Three-Dimensional Laser Doppler Velocimeter for the Measurement of Gas Flows," Eng. Rept 1678, Hayes International Corp., Birmingham, Ala., April 1970.

8. Hoffman, E. R. and Joubert, P. N. "Turbulent Line Vorticies," J. Fluid Mechanics, pp 395-411, Vol. 16, Part 3, July 1963.

Table I

Vortex Data Measurement Positions

Type Data	Position (cm) X	Y	Y Position (cm) From	To	Number Data Points
3-D	17.78	-0.167	11.43	0.762	114
3-D	35.56	-0.330	13.97	1.270	59
3-D	35.56	-0.167	13.97	1.778	102
3-D	35.56	0.020	13.33	3.810	68
3-D	35.56	0.170	13.97	1.270	118
3-D	35.56	0.210	13.97	5.080	83
3-D	35.56	0.480	13.97	1.270	92
1-D	35.56	0.020	10.15	6.700	60

Note: Wing Span = 17.78 cm (Data was taken at one and two wing spans behind the model)

Table II

Comparison of Perternate Characteristics of Vortex Data
in Reference 4 and that of the Author

Data Source	R_N	V_∞ (m/s)	Angle of Attack	Chord Length (cm)	Chord Lengths from Trailing Edge	Wing Type
Rorke*	460,000	73	6°	10.8	2.0	NACA 0012
Rorke*	450,000	72	6°	10.8	5.0	NACA 0012
Author	360,000	84	6°	6.6	2.7	6% biconvex
Author	360,000	84	6°	6.6	5.4	6% biconvex

* Ref. 4

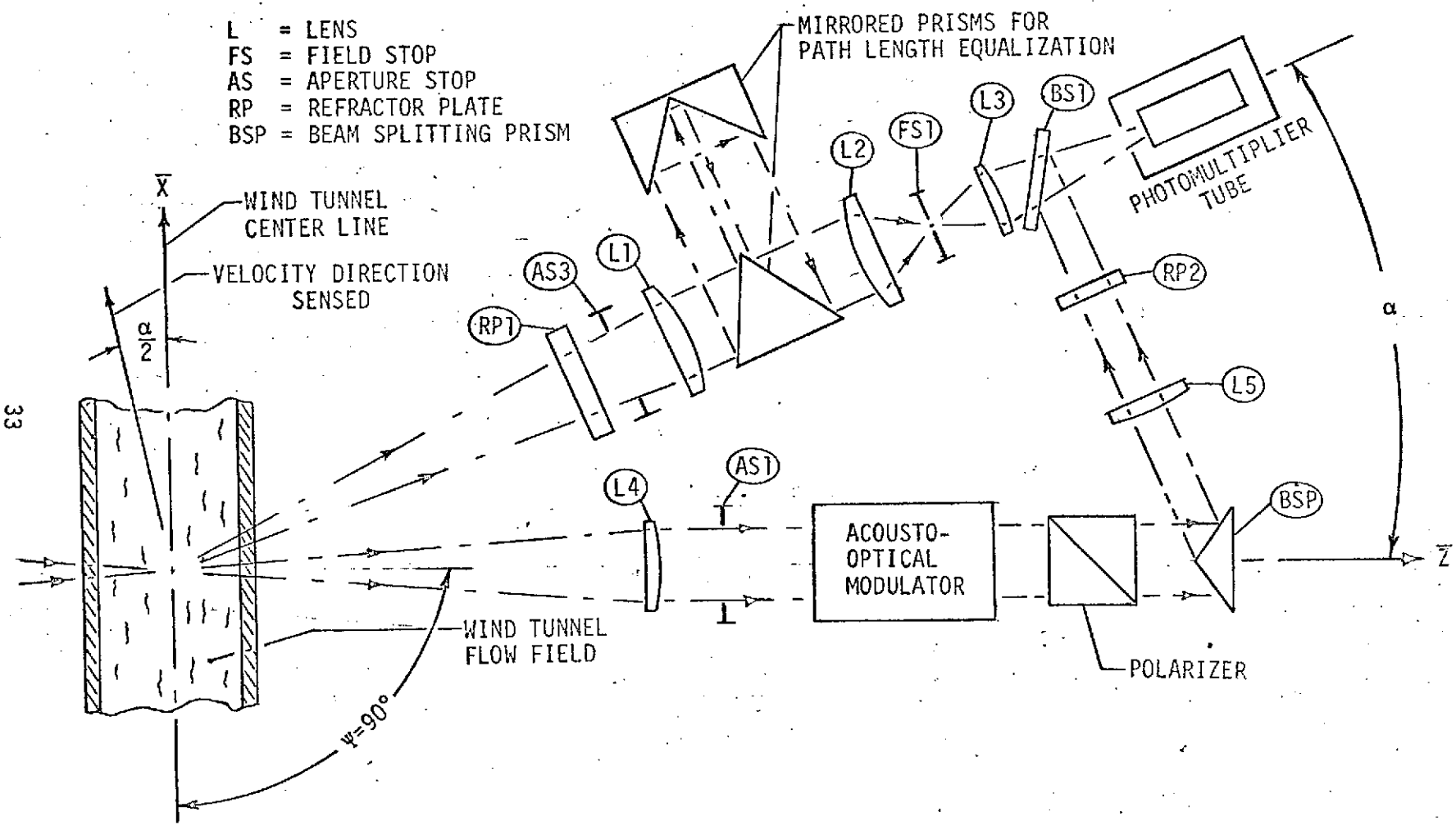

FIGURE 1. SCHEMATIC OF ONE COMPONENT OF THE THREE-DIMENSIONAL LDV INSTRUMENT

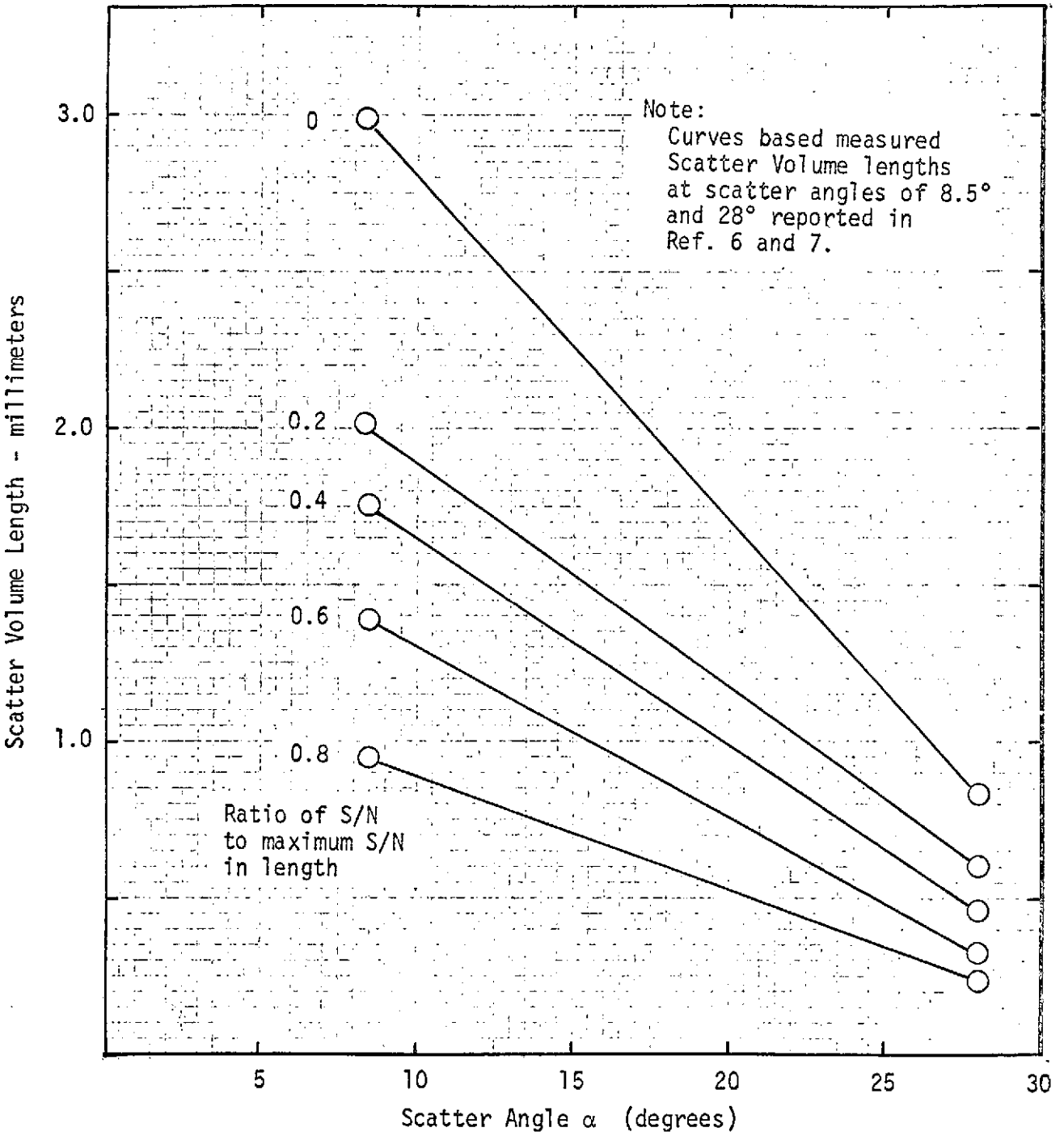

Fig. 2 Scatter Volume Length Variation with Scatter Angle for 3-D LDV Instrument

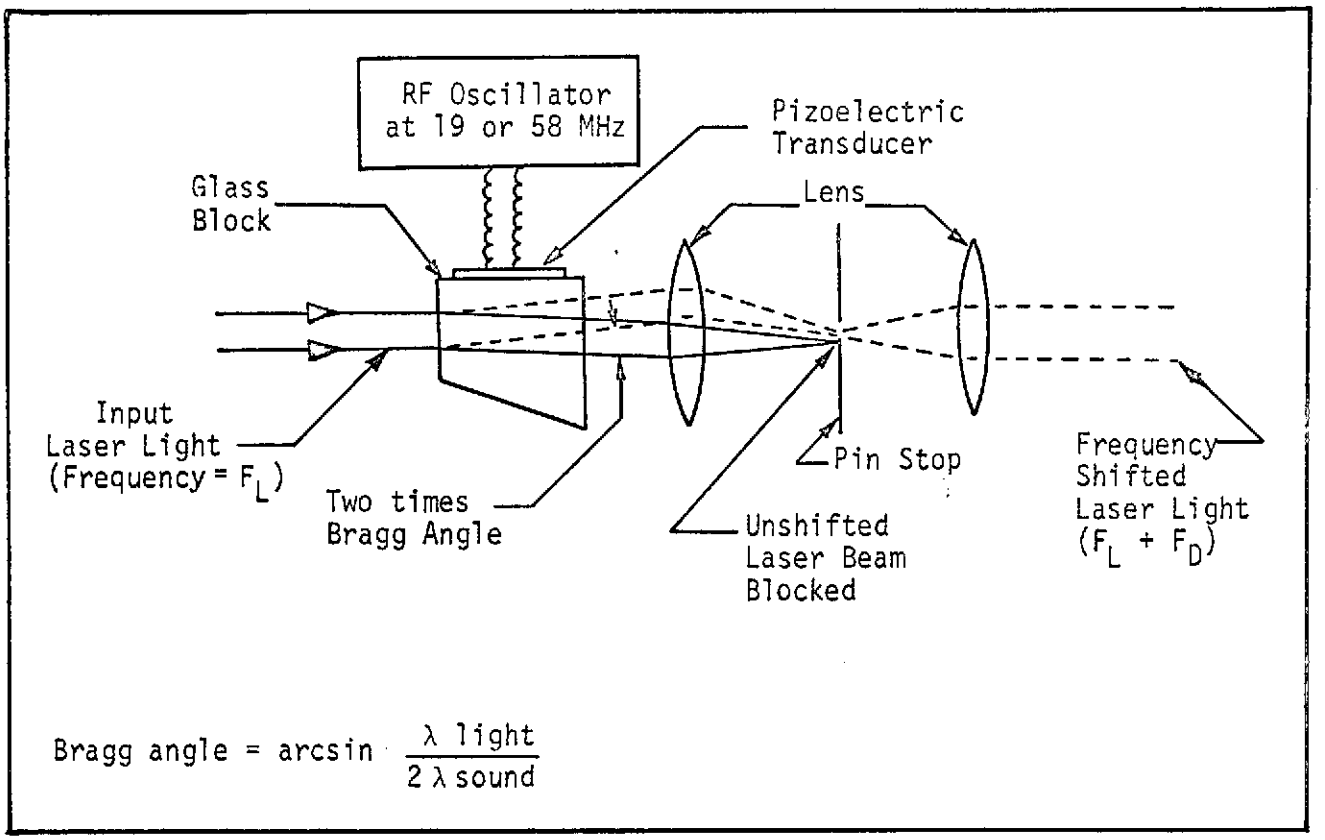

Figure 3 Schematic of Acousto-Optic-Modulator

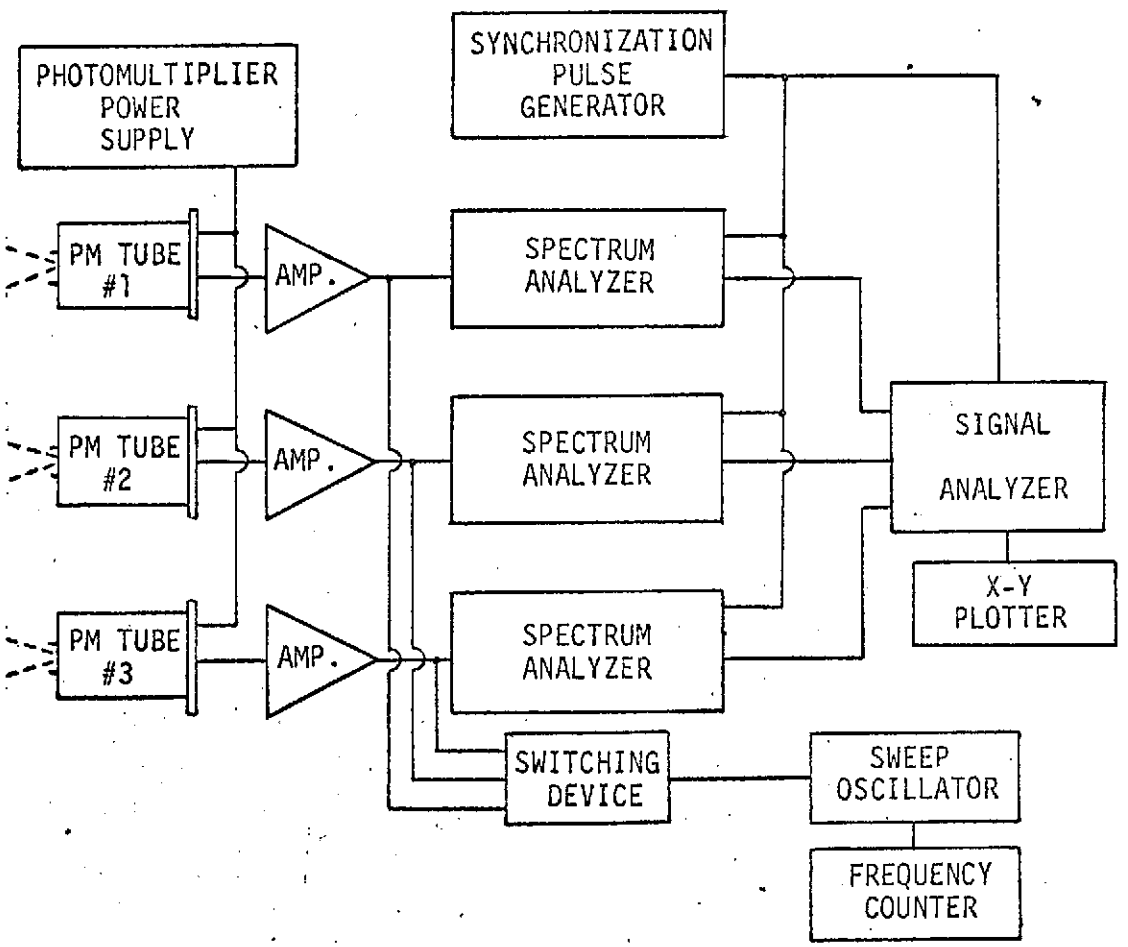

FIGURE 4 SCHEMATIC OF ELECTRONIC NETWORK FOR DATA ACQUISITION AND IDENTIFICATION AT THE MSFC 7 X 7-INCH WIND TUNNEL TESTS

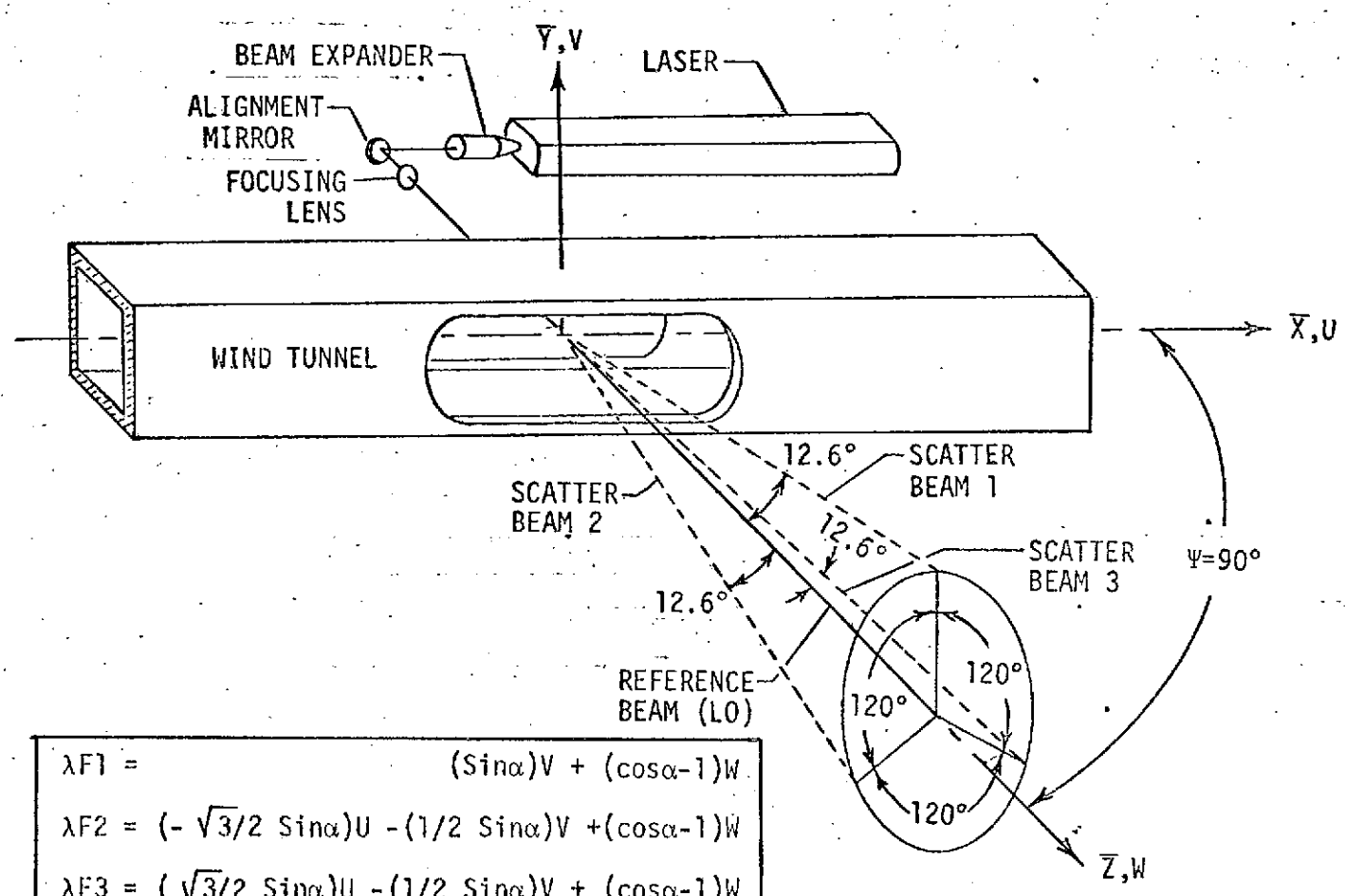

$$\lambda F1 = (\sin\alpha)V + (\cos\alpha - 1)W$$

$$\lambda F2 = (-\sqrt{3}/2\ \sin\alpha)U - (1/2\ \sin\alpha)V + (\cos\alpha - 1)W$$

$$\lambda F3 = (\sqrt{3}/2\ \sin\alpha)U - (1/2\ \sin\alpha)V + (\cos\alpha - 1)W$$

FIGURE 5 SCHEMATIC OF THE THREE DIMENSIONAL LASER DOPPLER VELOCIMETER AND ITS ANGULAR ALIGNMENT RELATIVE TO A WIND TUNNEL

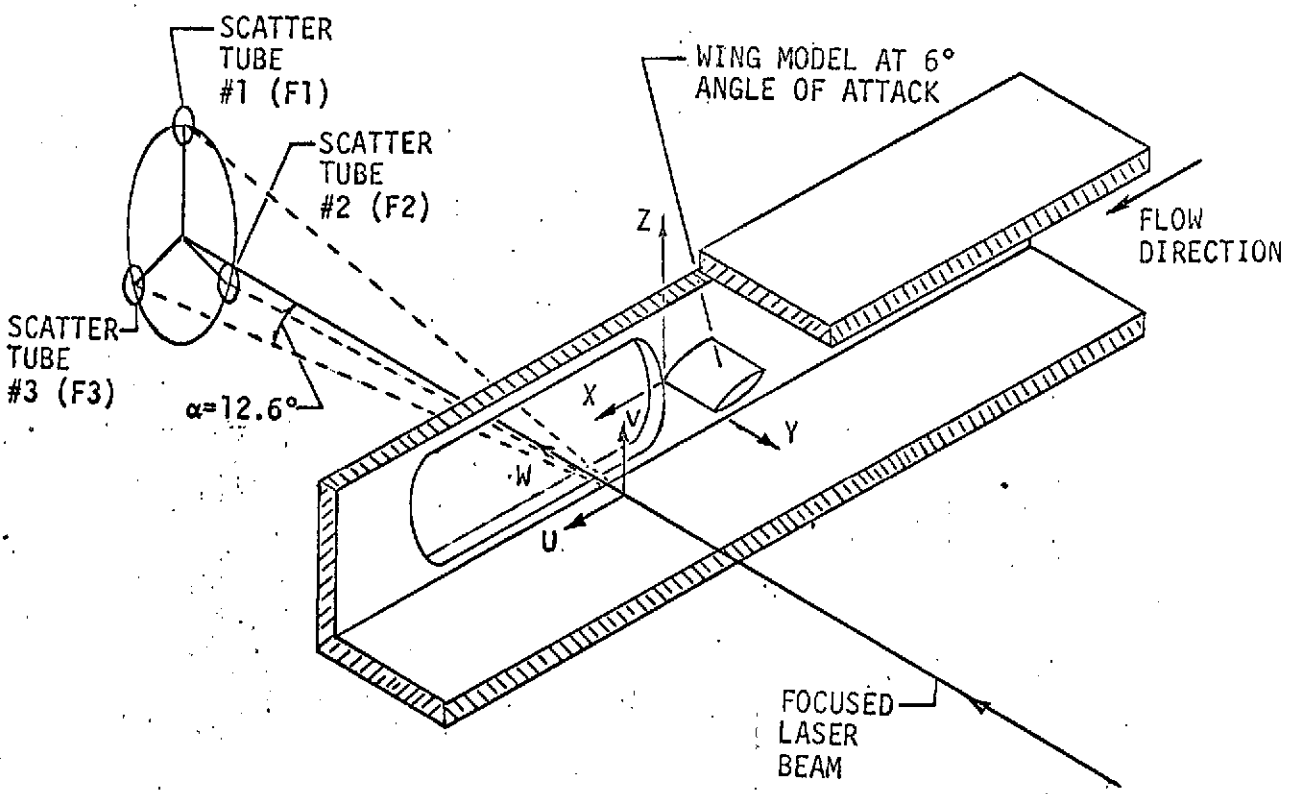

FIGURE 6 SKETCH OF LDV INSTRUMENTATION ARRANGEMENT RELATIVE TO WIND TUNNEL COORDINATE SYSTEM

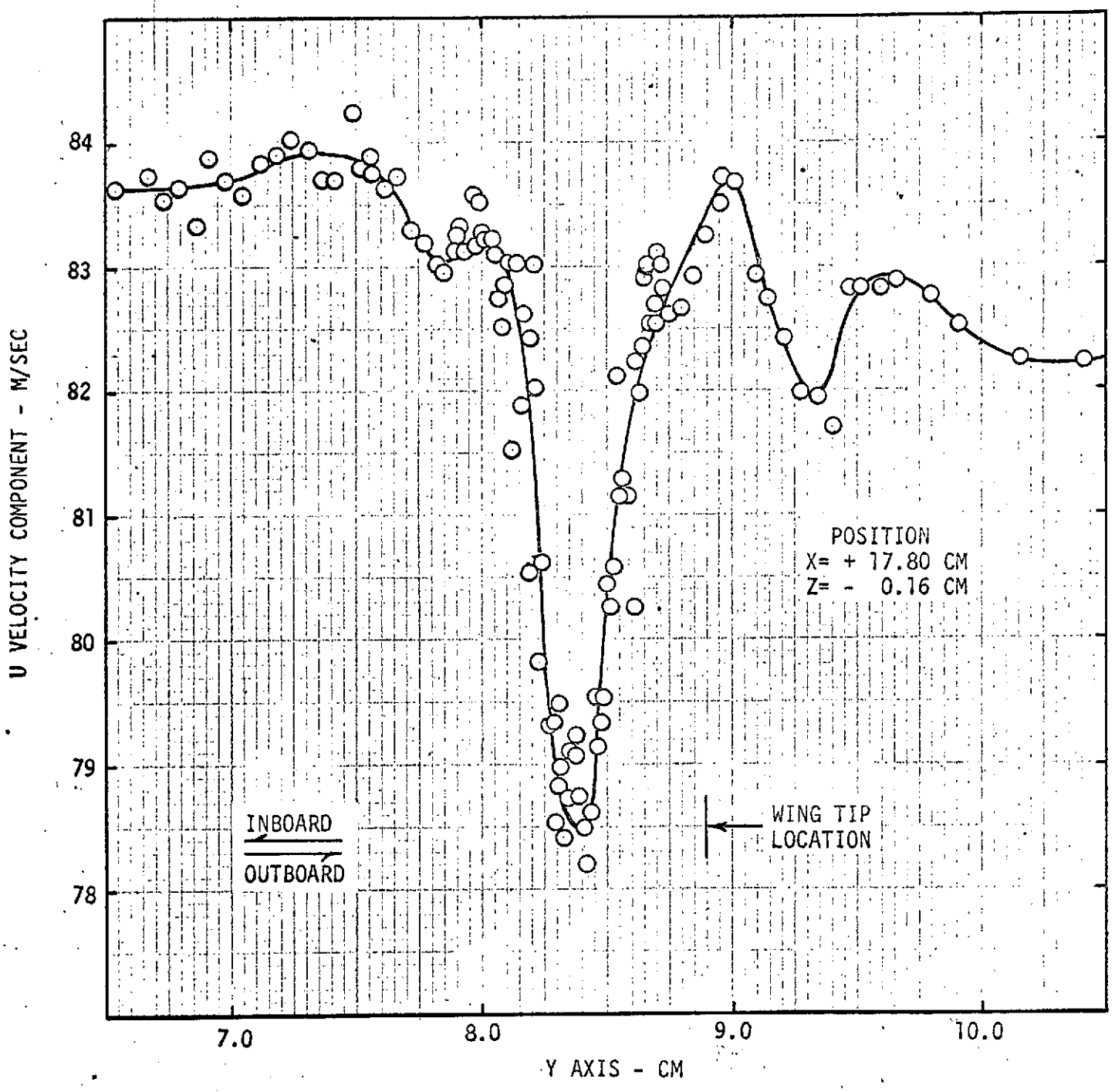

FIGURE 7 U VELOCITY COMPONENT PROFILE IN A WING TIP VORTEX

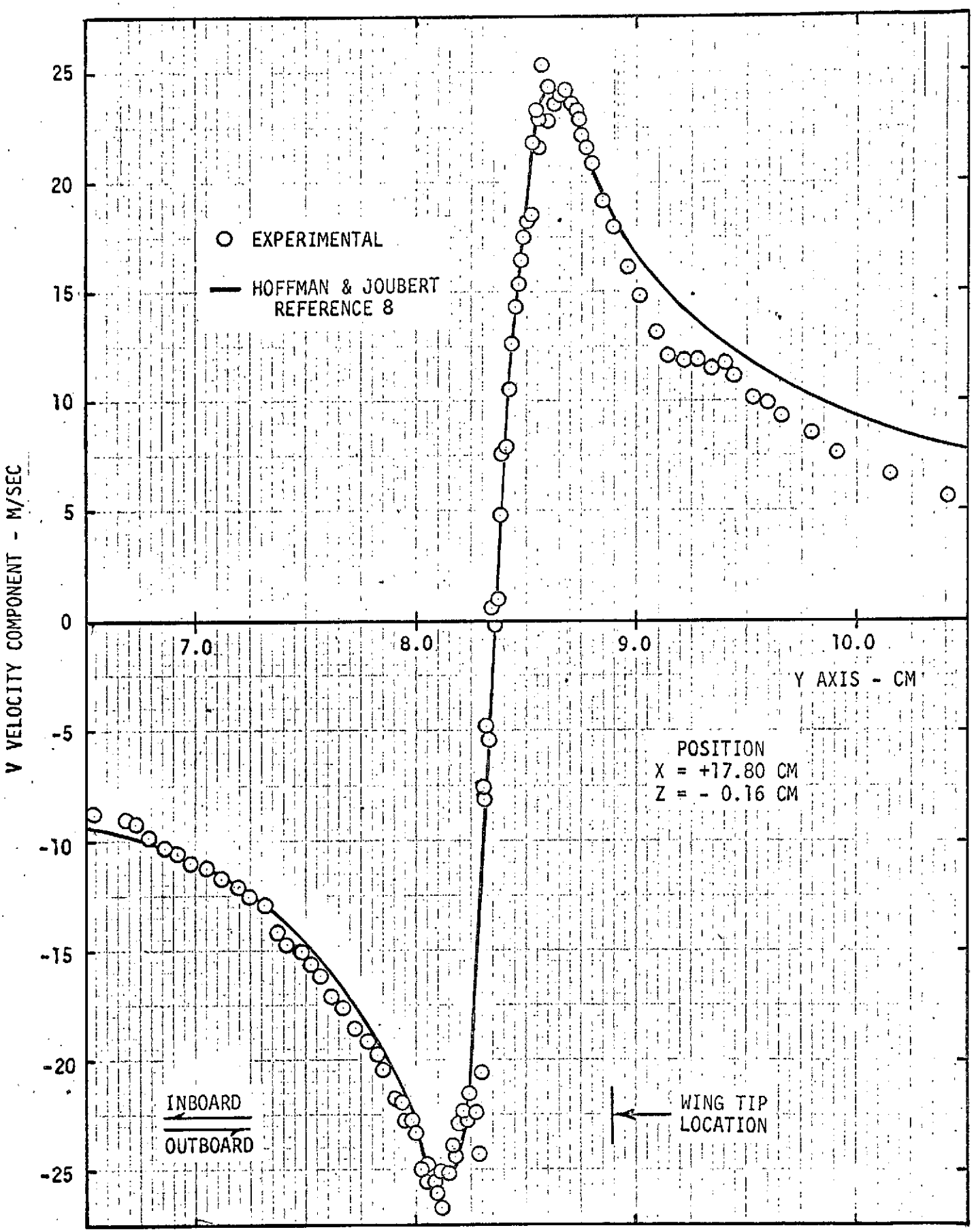

FIGURE 8 V VELOCITY COMPONENT PROFILE IN A WING TIP VORTEX

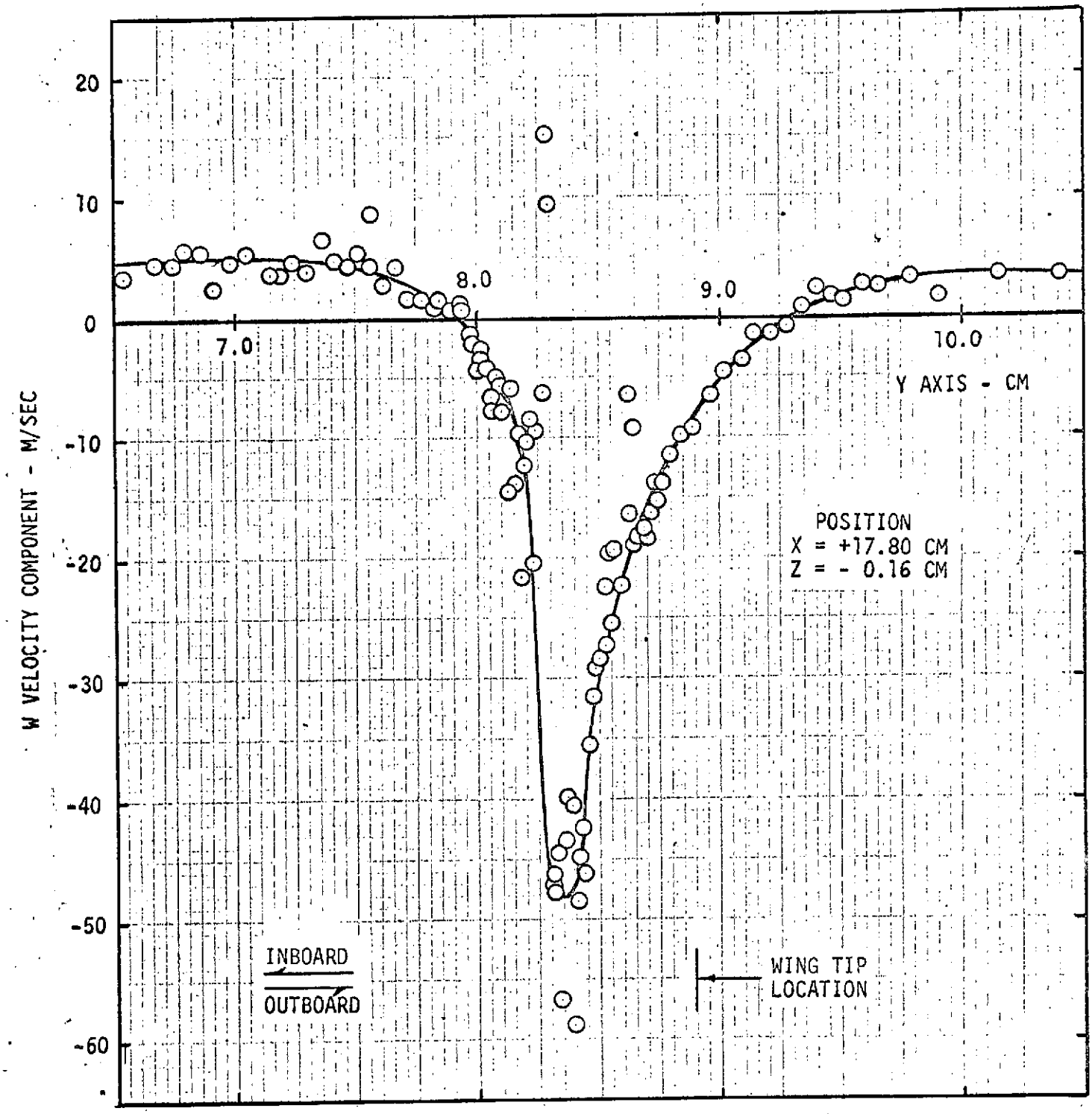

FIGURE 9 W VELOCITY COMPONENT PROFILE IN A WING TIP VORTEX

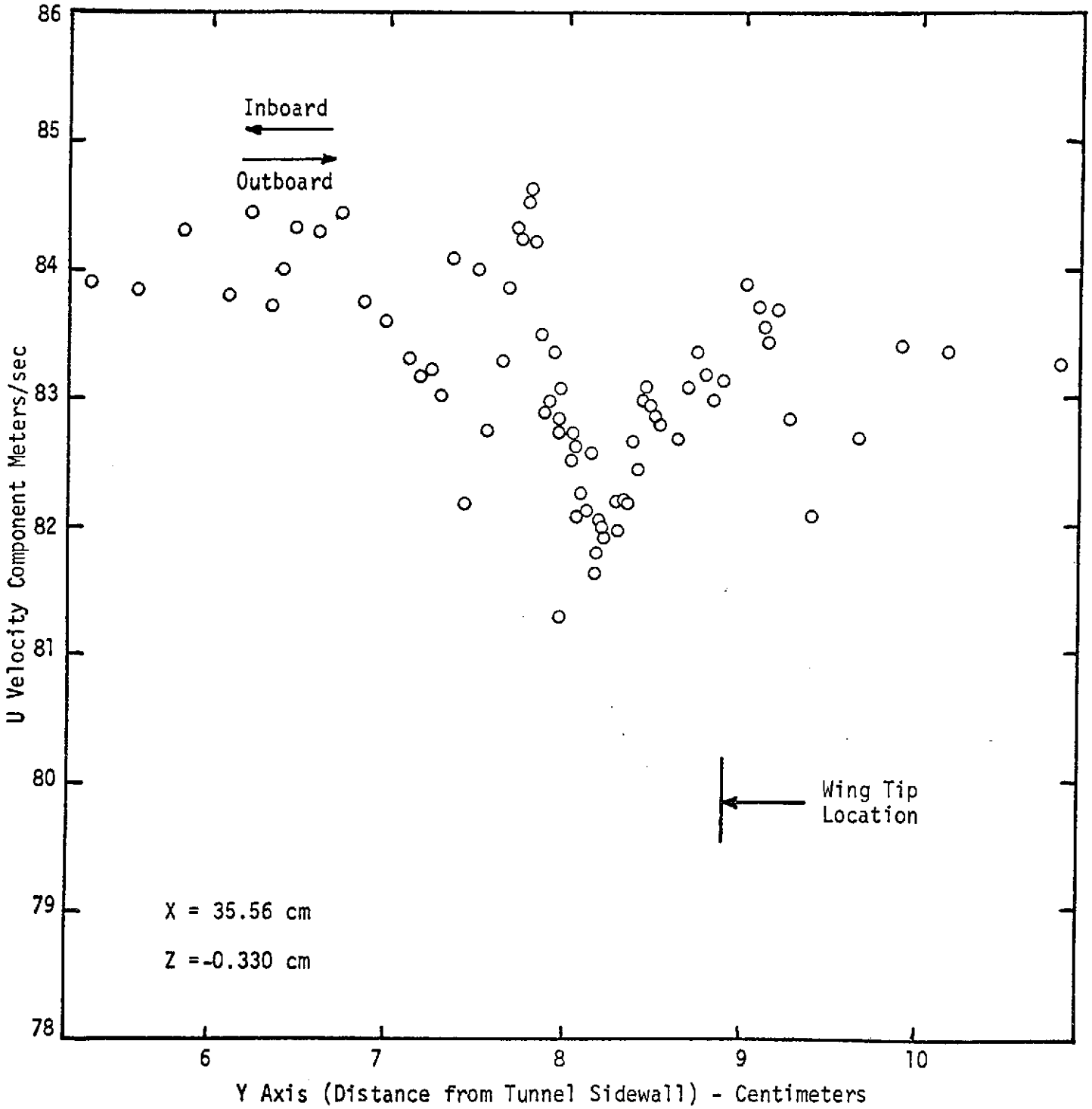

Fig. 10 U Velocity Component Distribution in Wing Tip Vortex

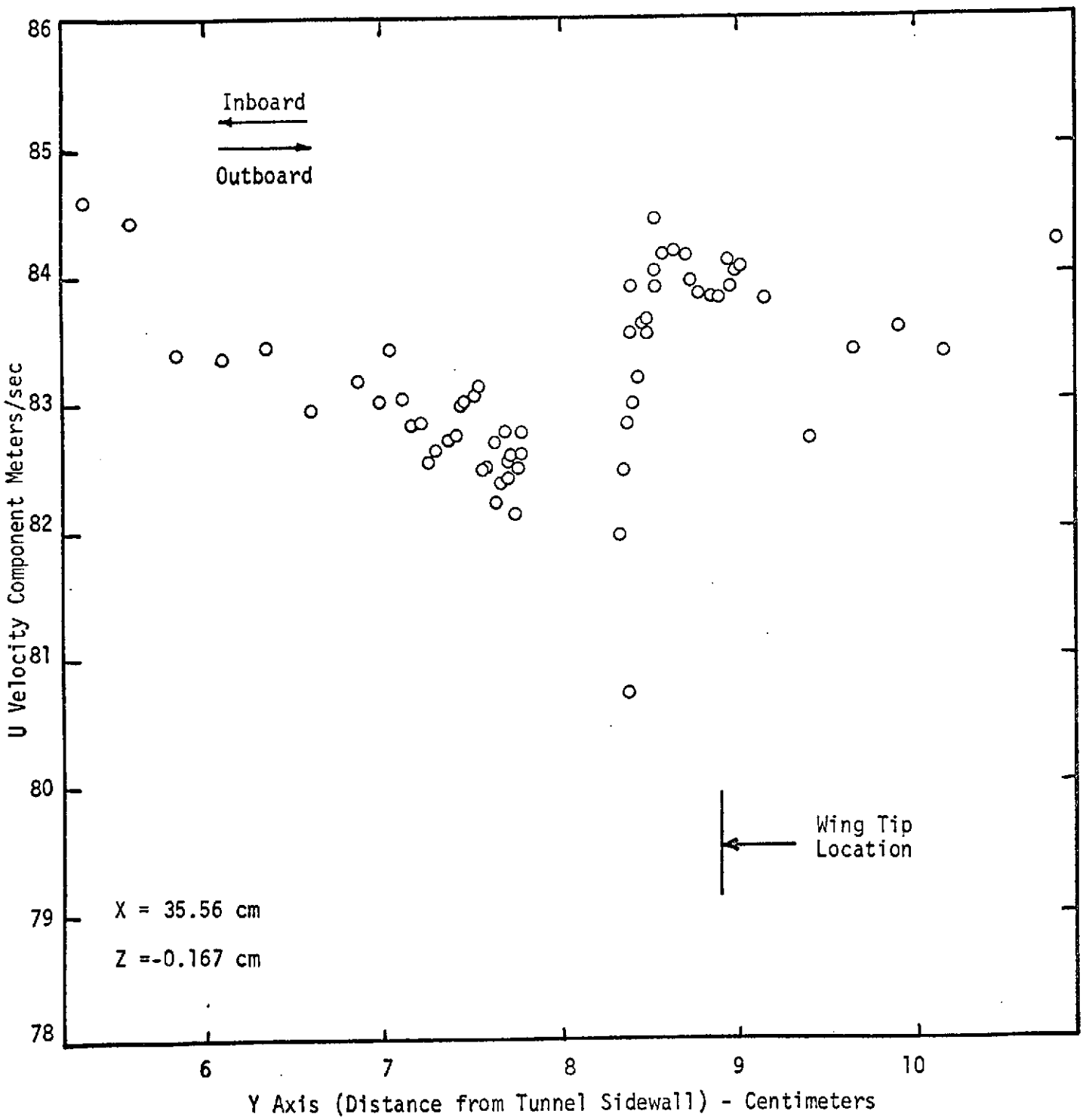

Fig. 11 U Velocity Component Distribution in Wing Tip Vortex

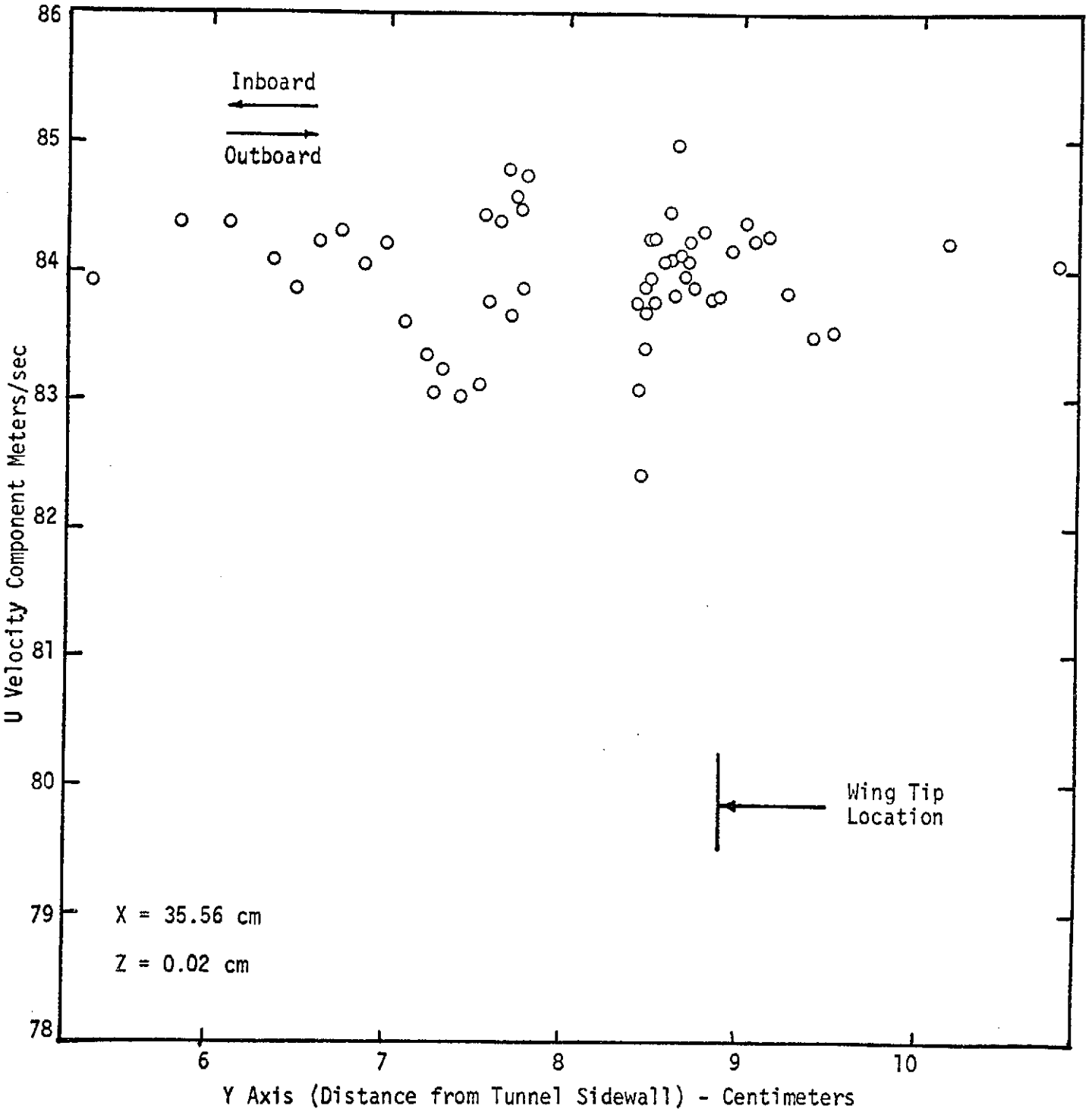

Fig. 12 U Velocity Component Distribution in Wing Tip Vortex

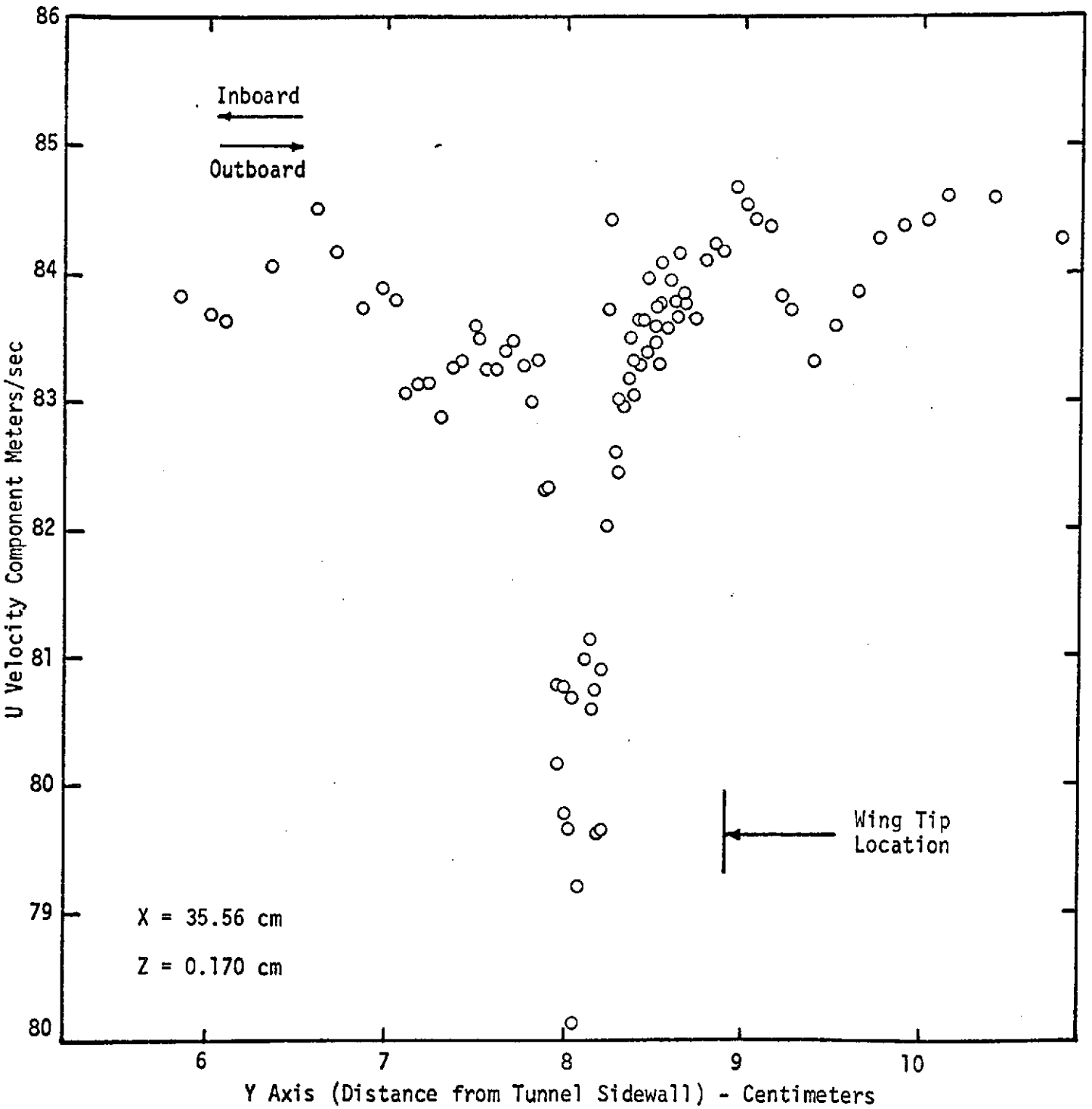

Fig. 13 U Velocity Component Distribution in Wing Tip Vortex

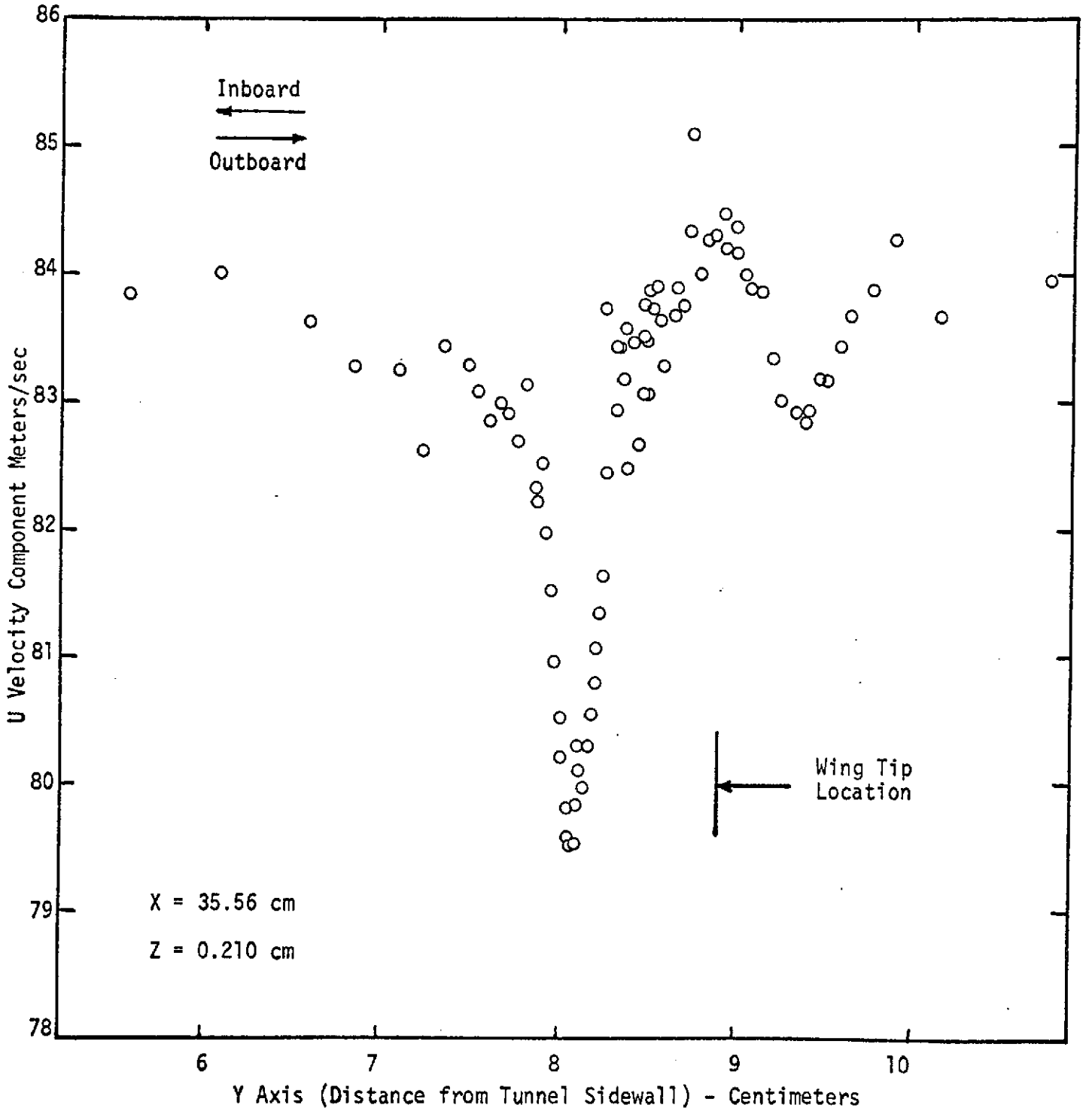

Fig. 14 U Velocity Component Distribution in Wing Tip Vortex

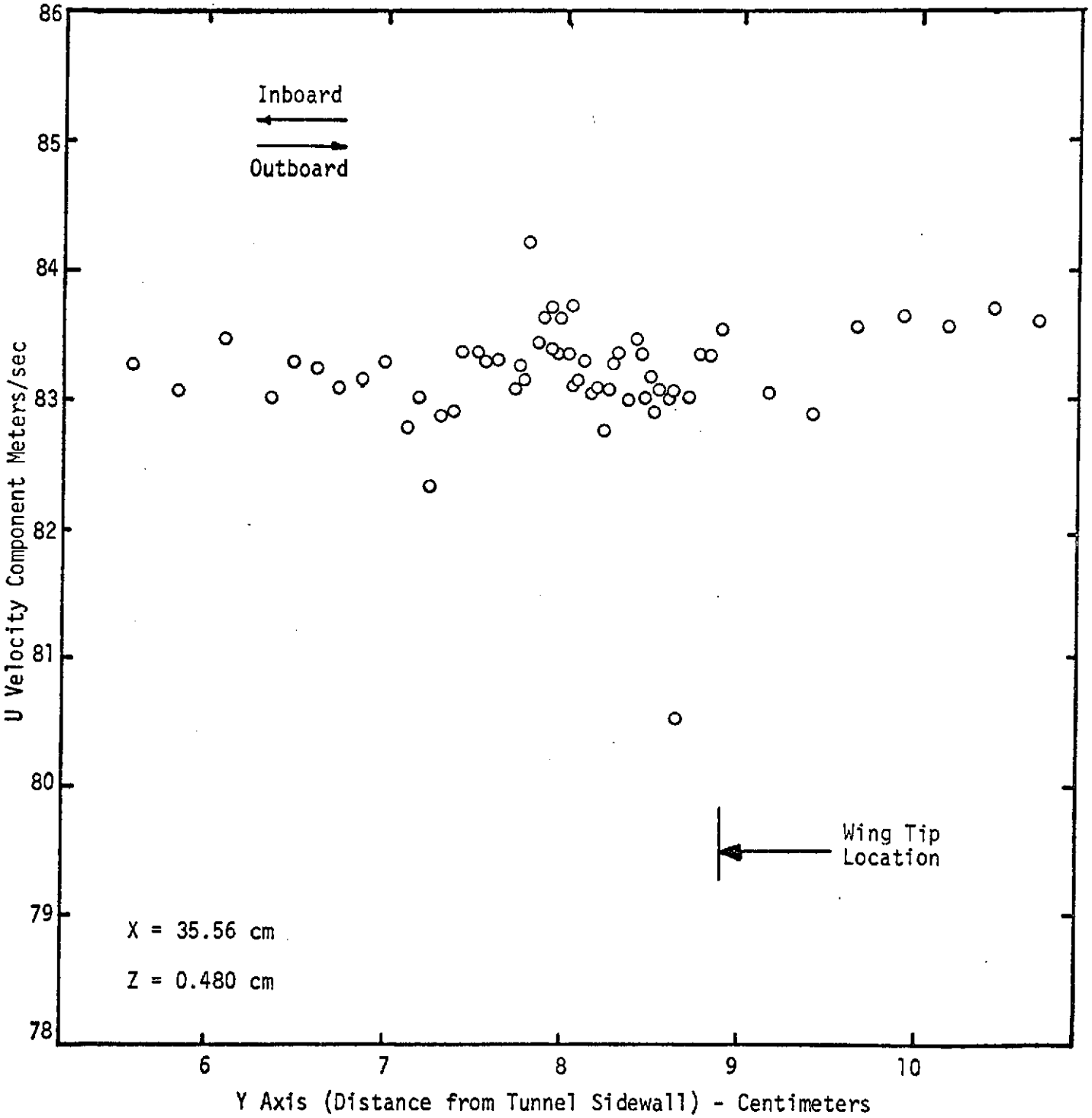

Fig. 15 U Velocity Component Distribution in Wing Tip Vortex

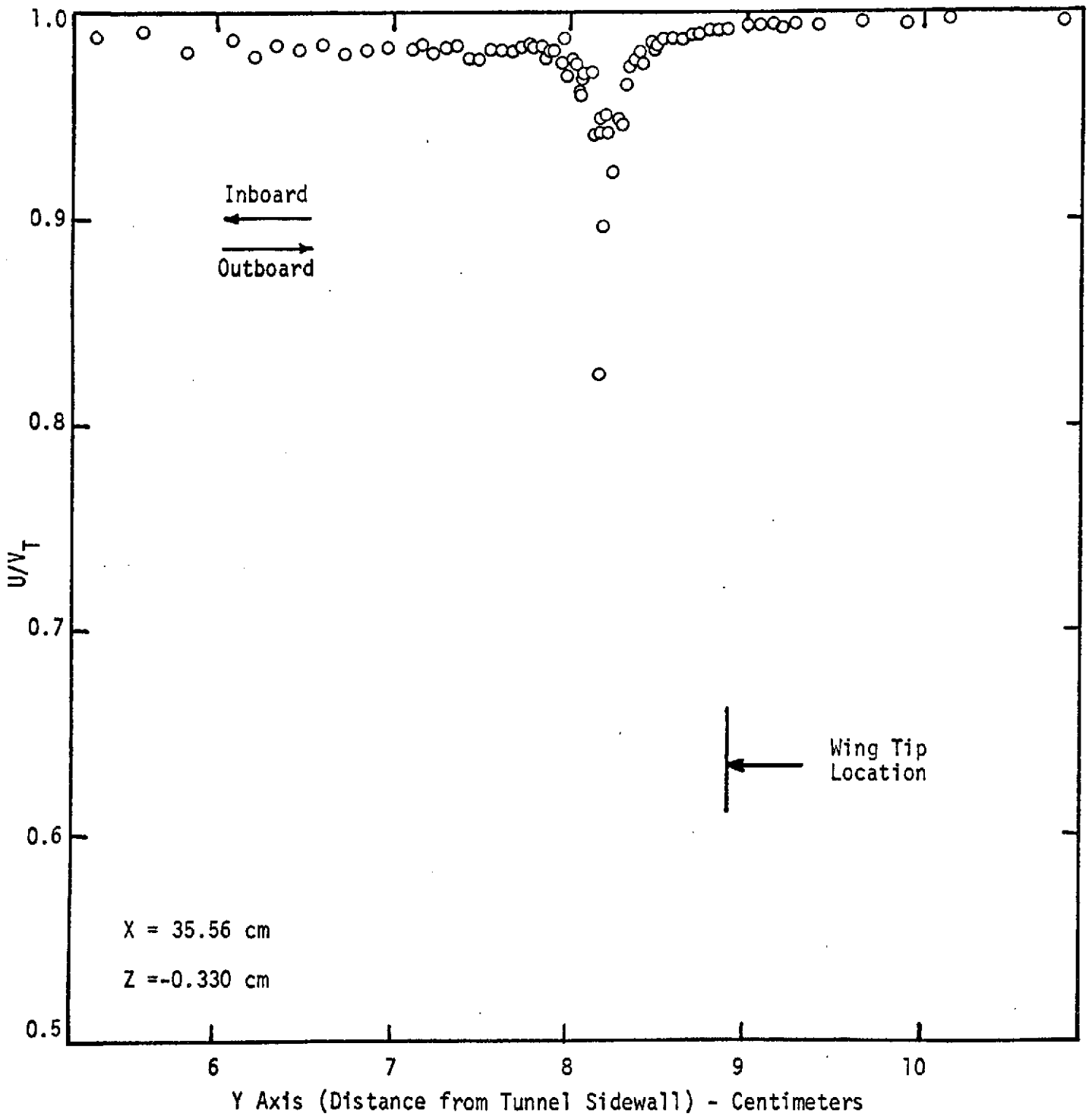

Fig. 16 U Velocity Component Distribution in Wing Tip Vortex

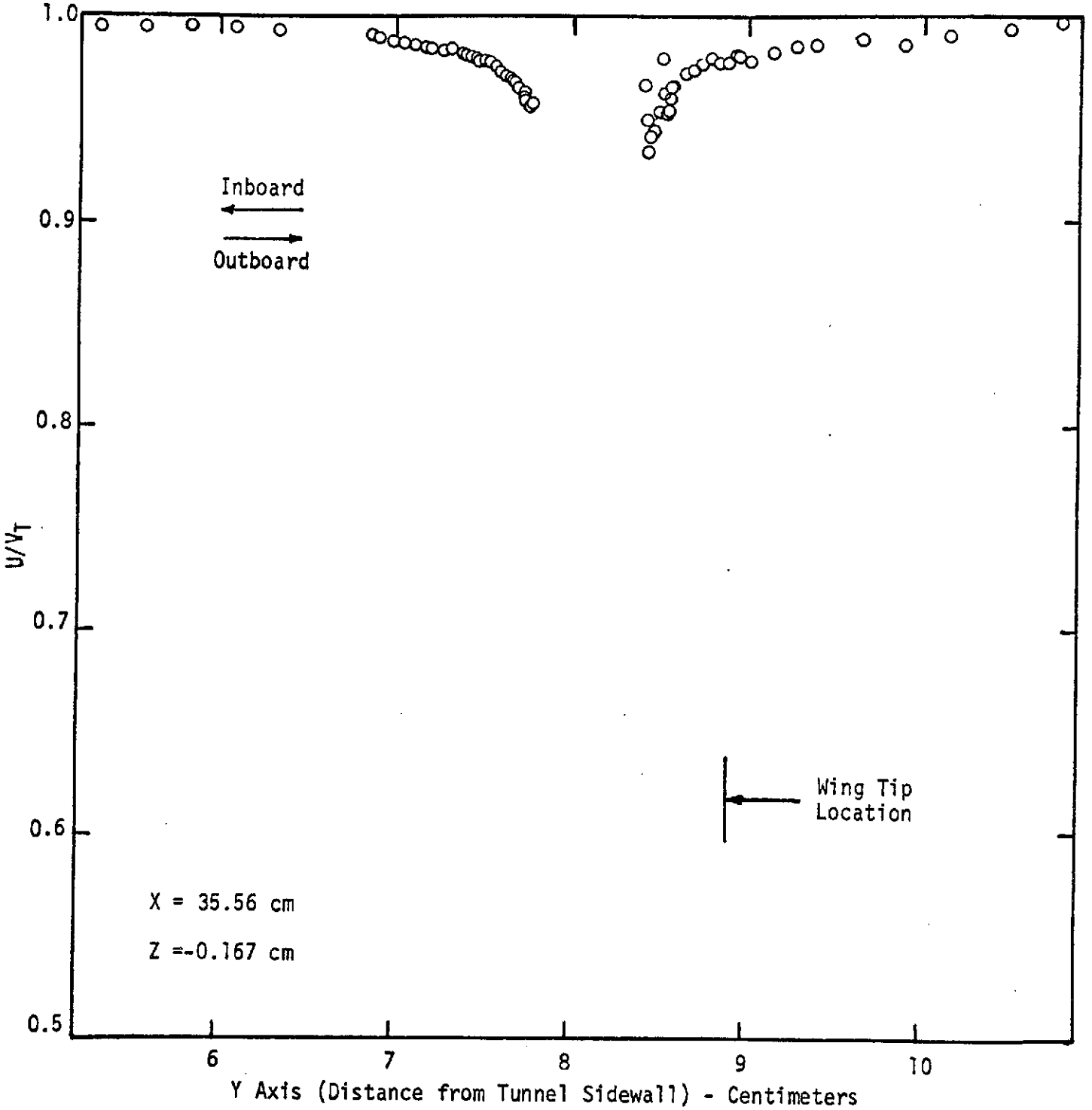

Fig. 17 U Velocity Component Distribution in Wing Tip Vortex

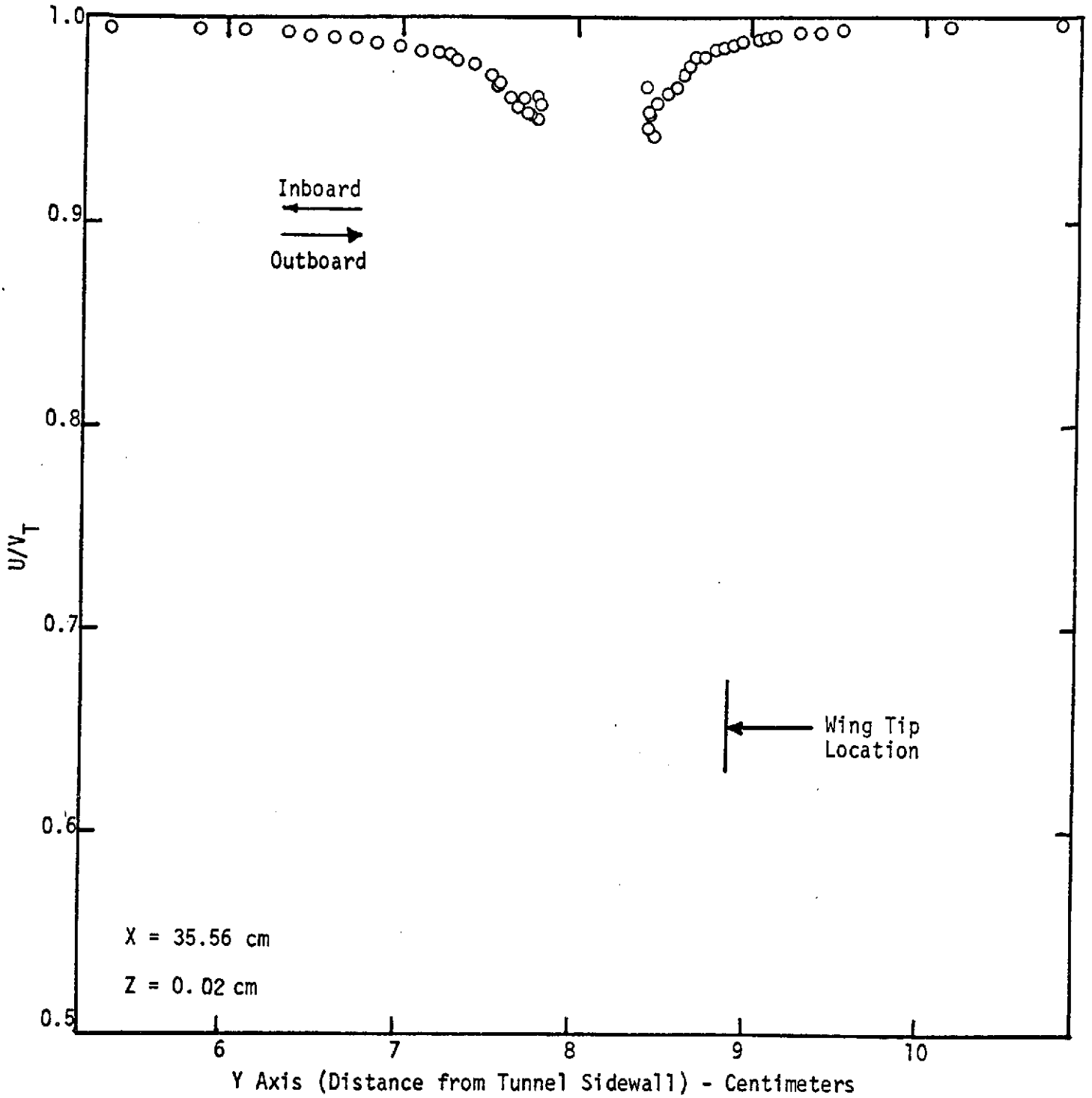

Fig. 18 U Velocity Component Distribution in Wing Tip Vortex

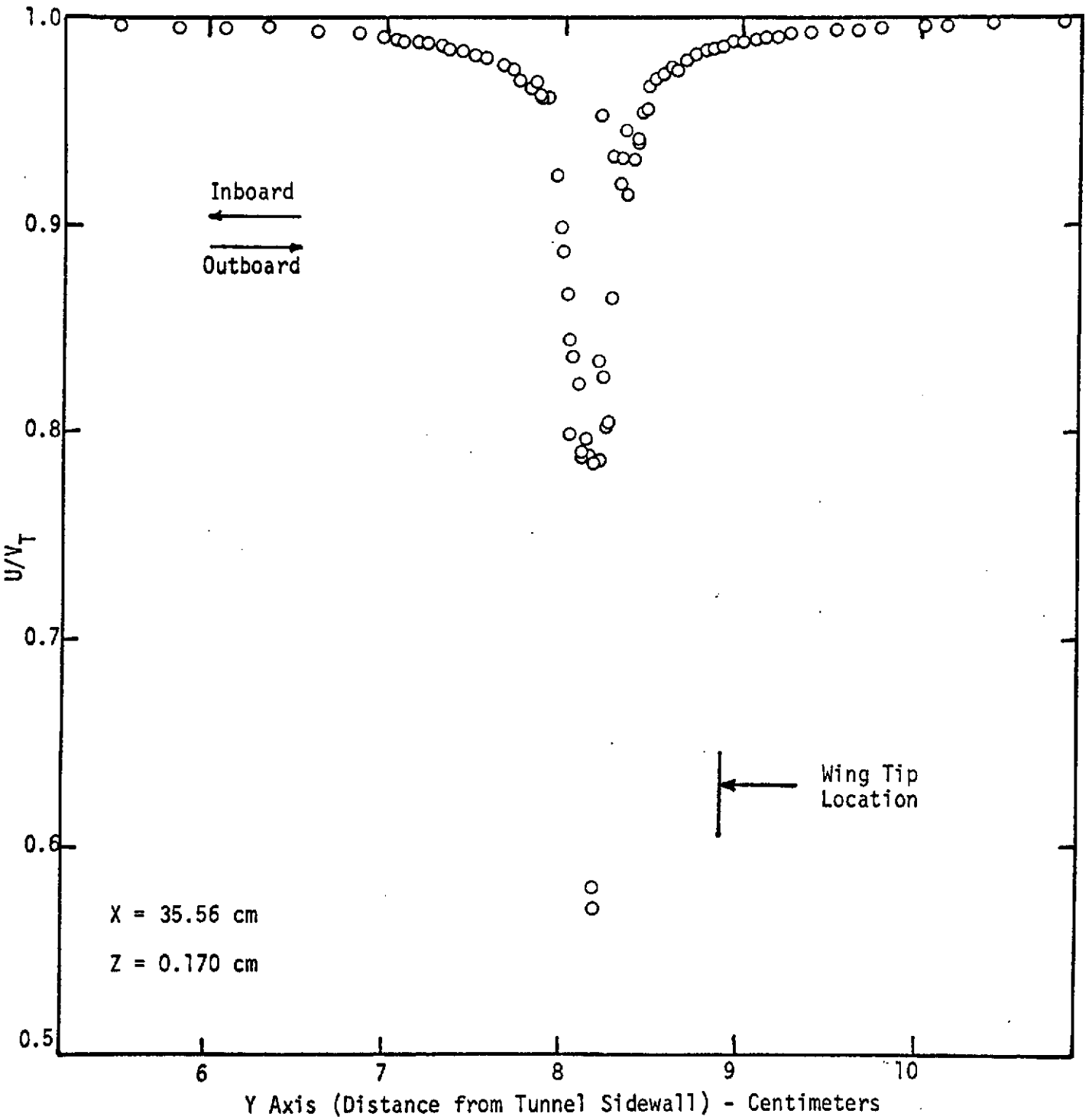

Fig. 19 U Velocity Component Distribution in Wing Tip Vortex

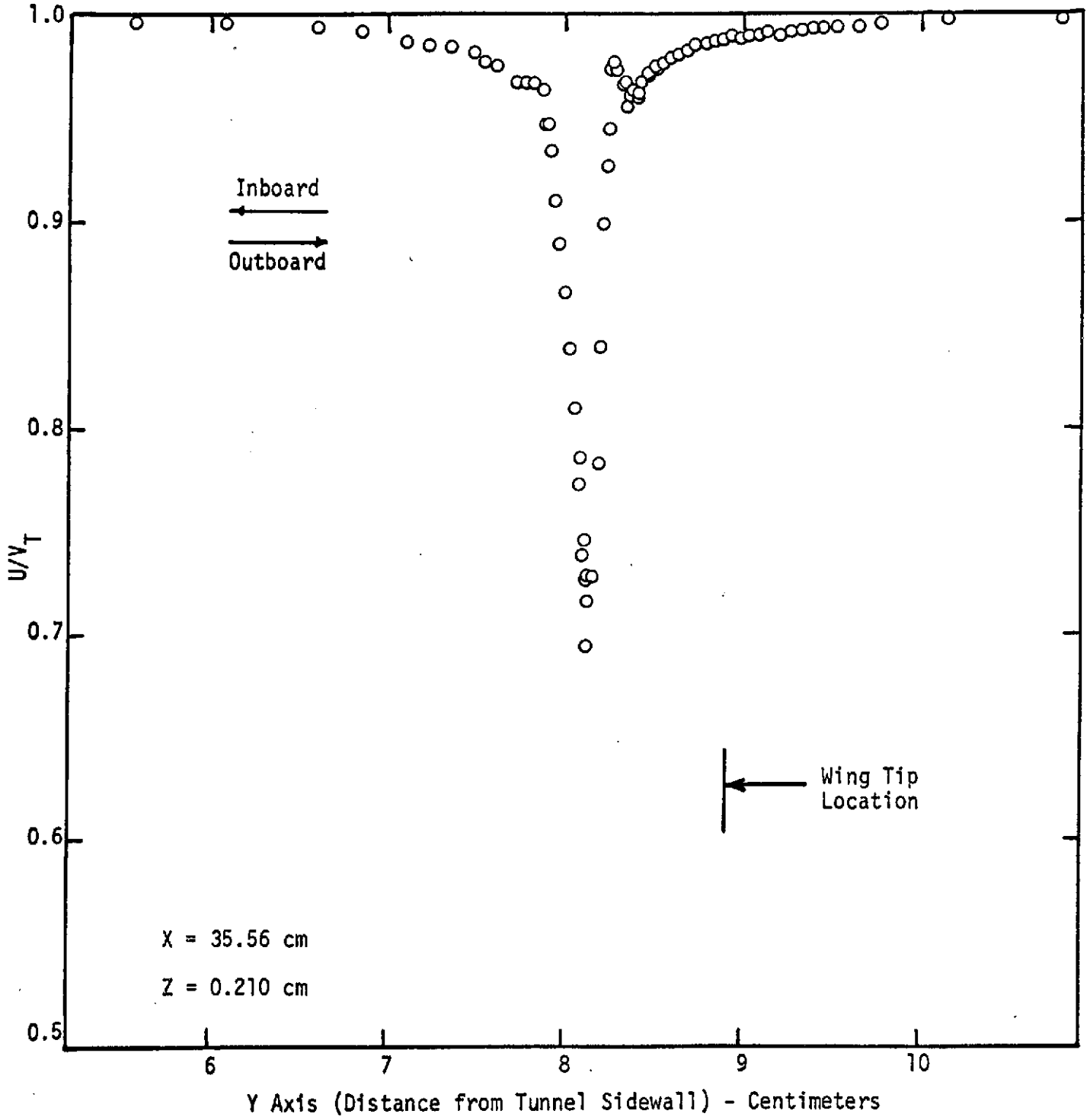

Fig. 20 U Velocity Component Distribution in Wing Tip Vortex

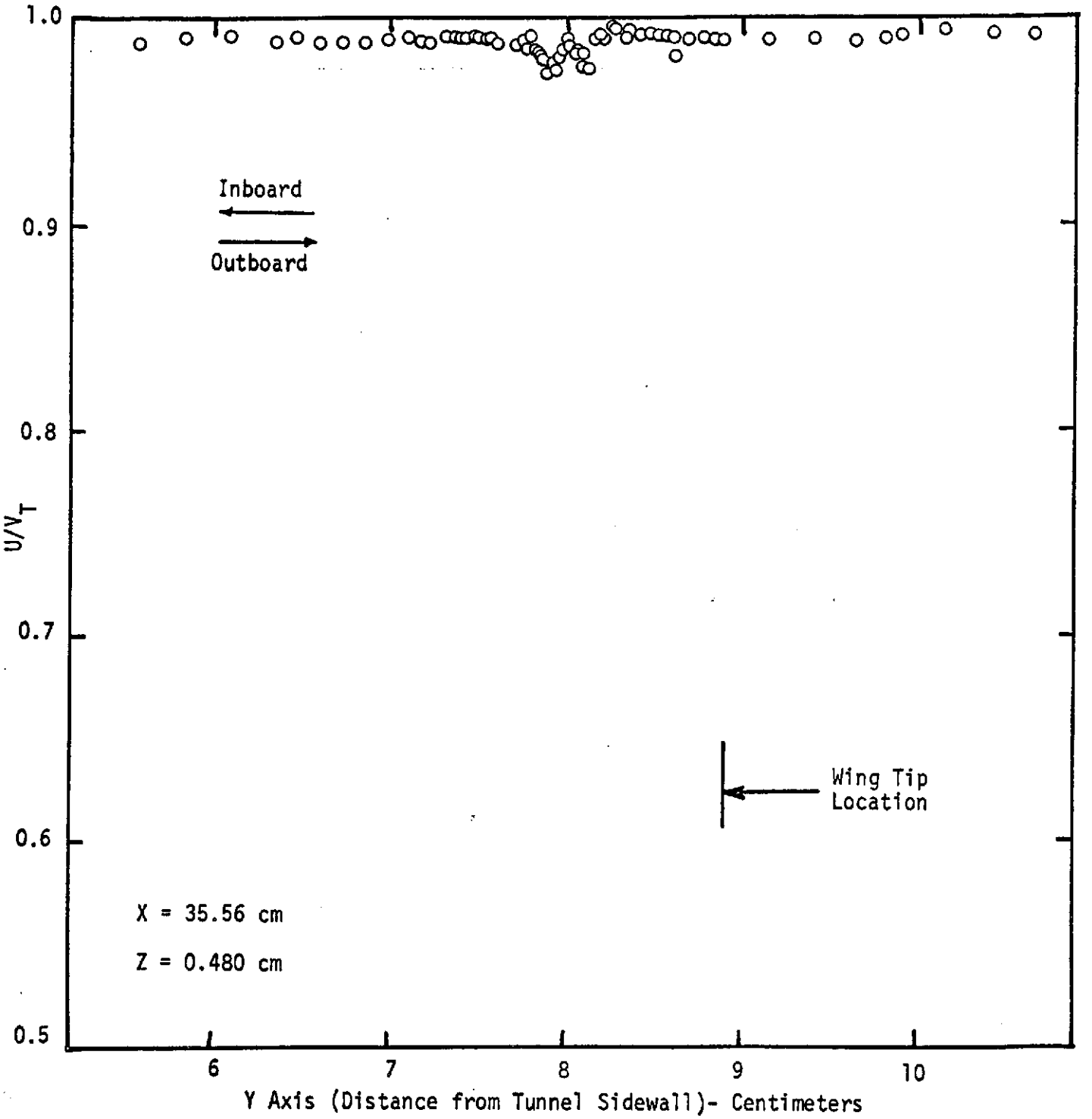

Fig.21 U Velocity Component Distribution in Wing Tip Vortex

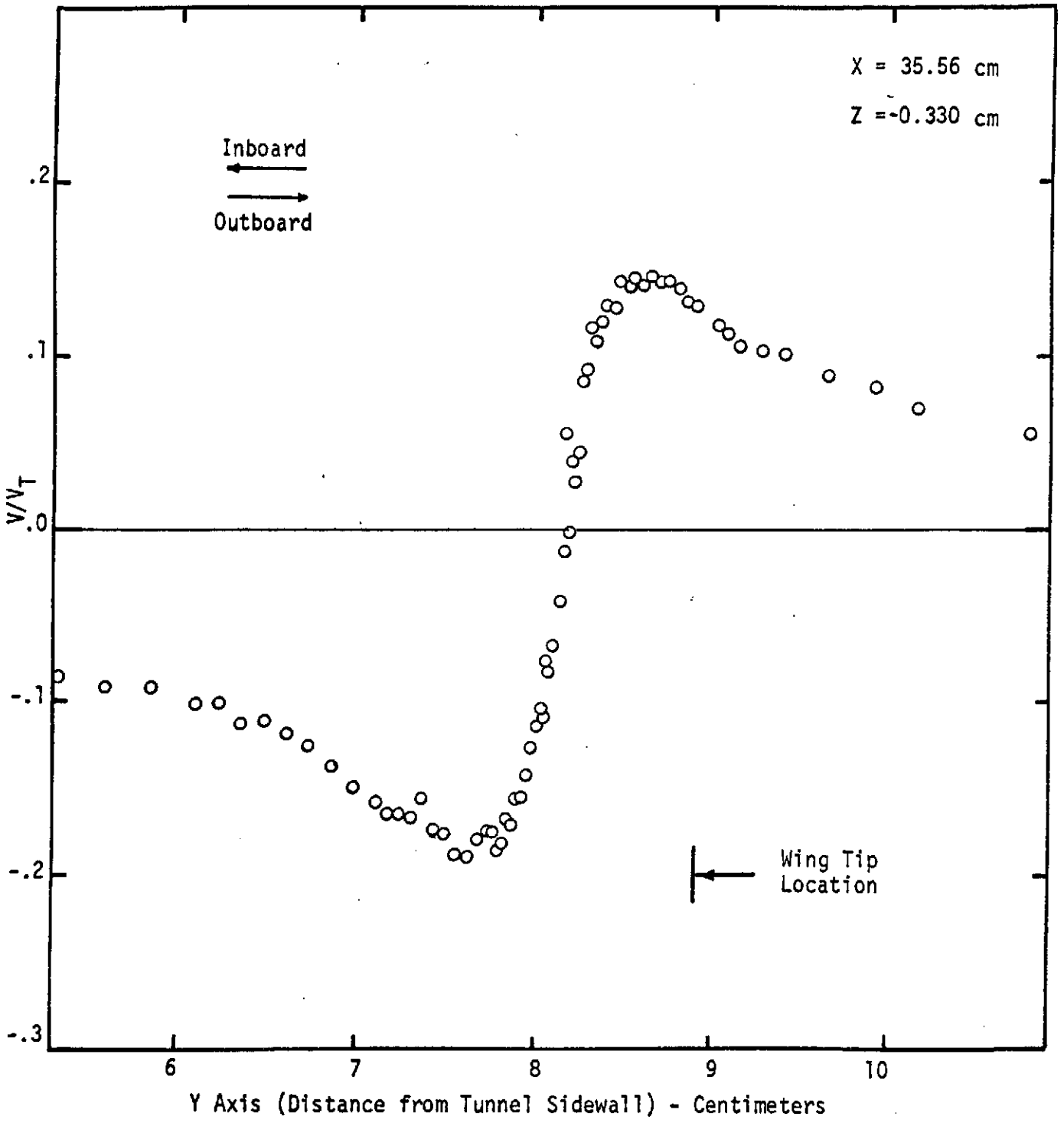

Fig. 22 V Velocity Component Distribution in Wing Tip Vortex

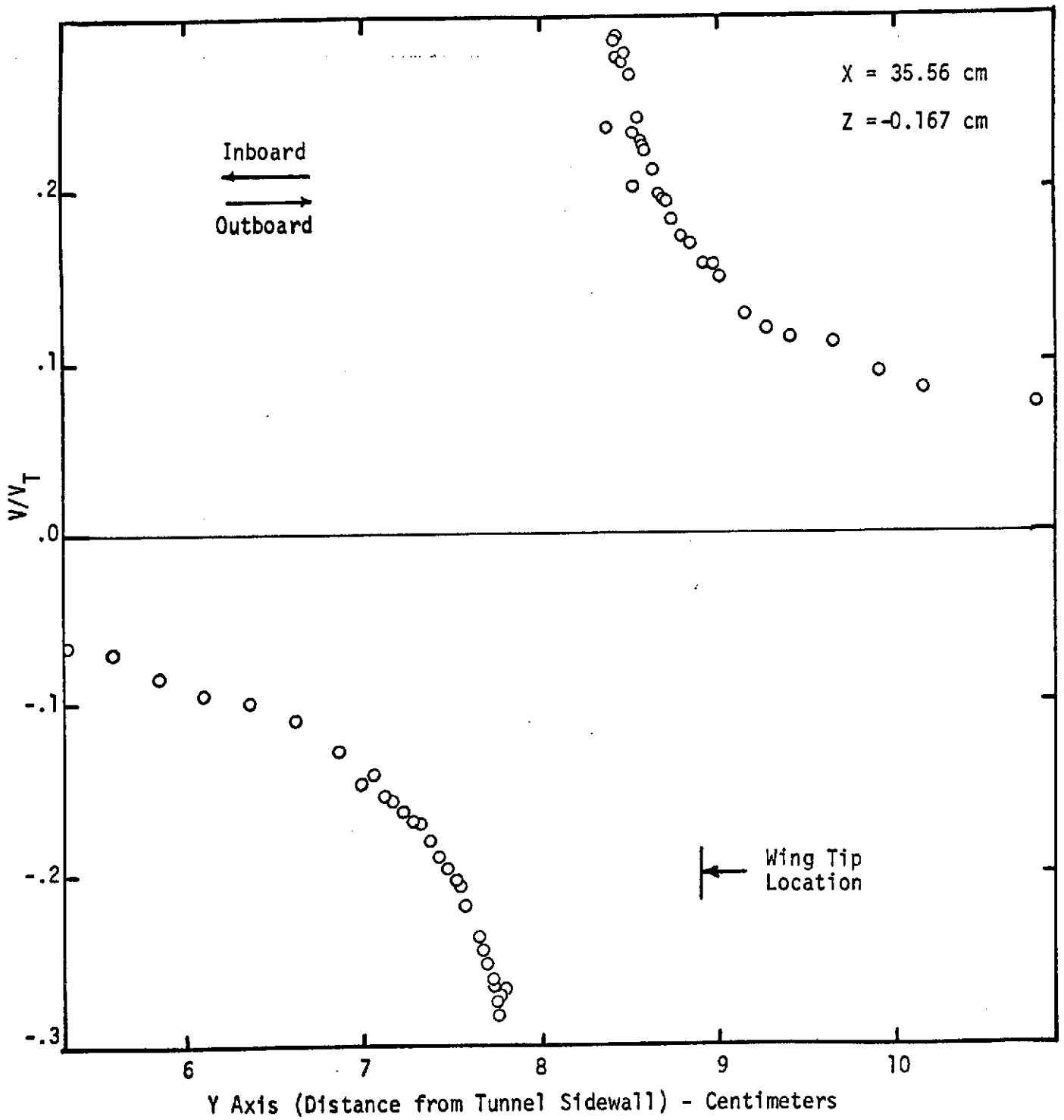

Fig. 23 V Velocity Component Distribution in Wing Tip Vortex

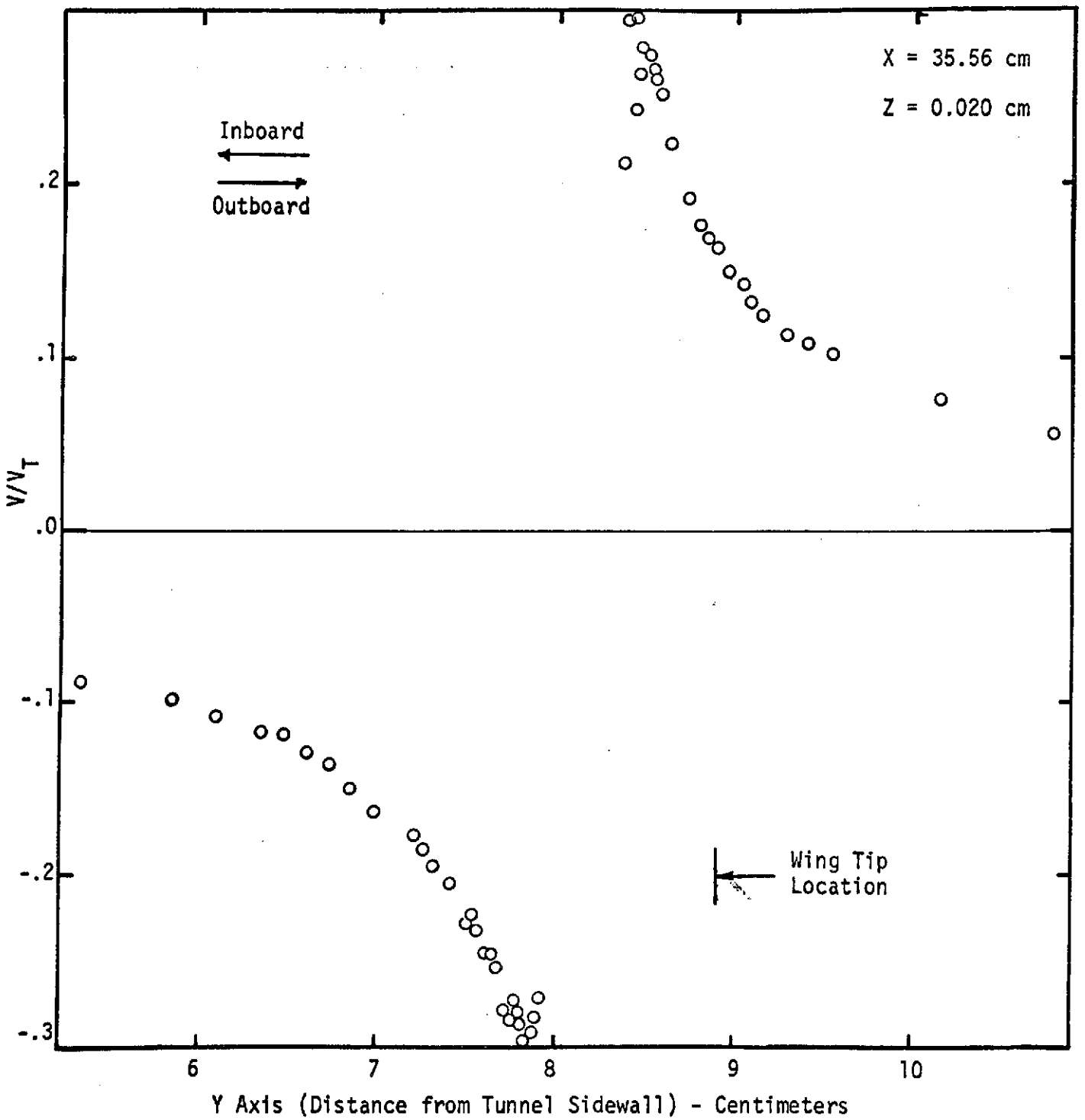

Fig. 24 V Velocity Component Distribution in Wing Tip Vortex

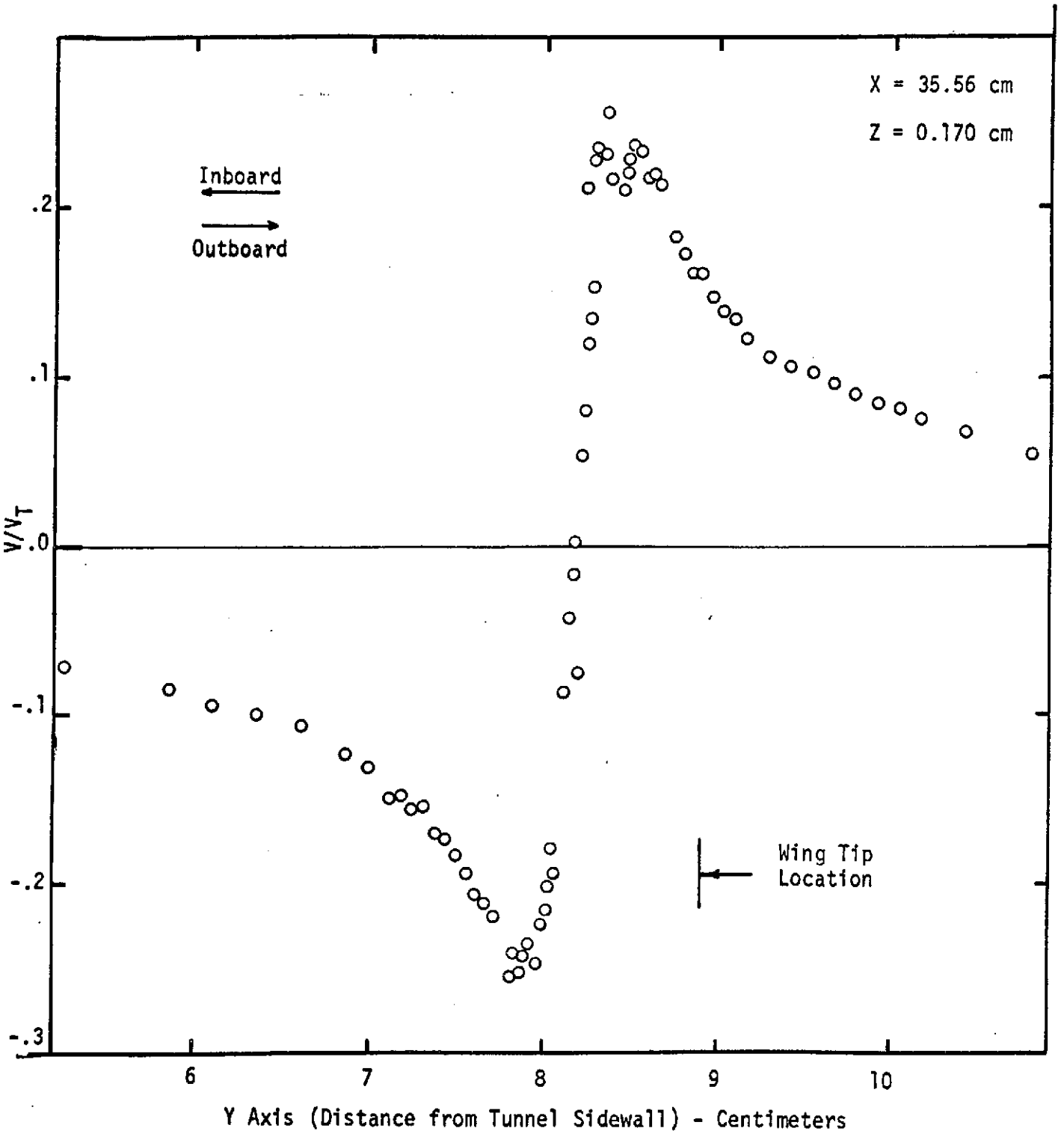

Fig. 25 V Velocity Component Distribution in Wing Tip Vortex

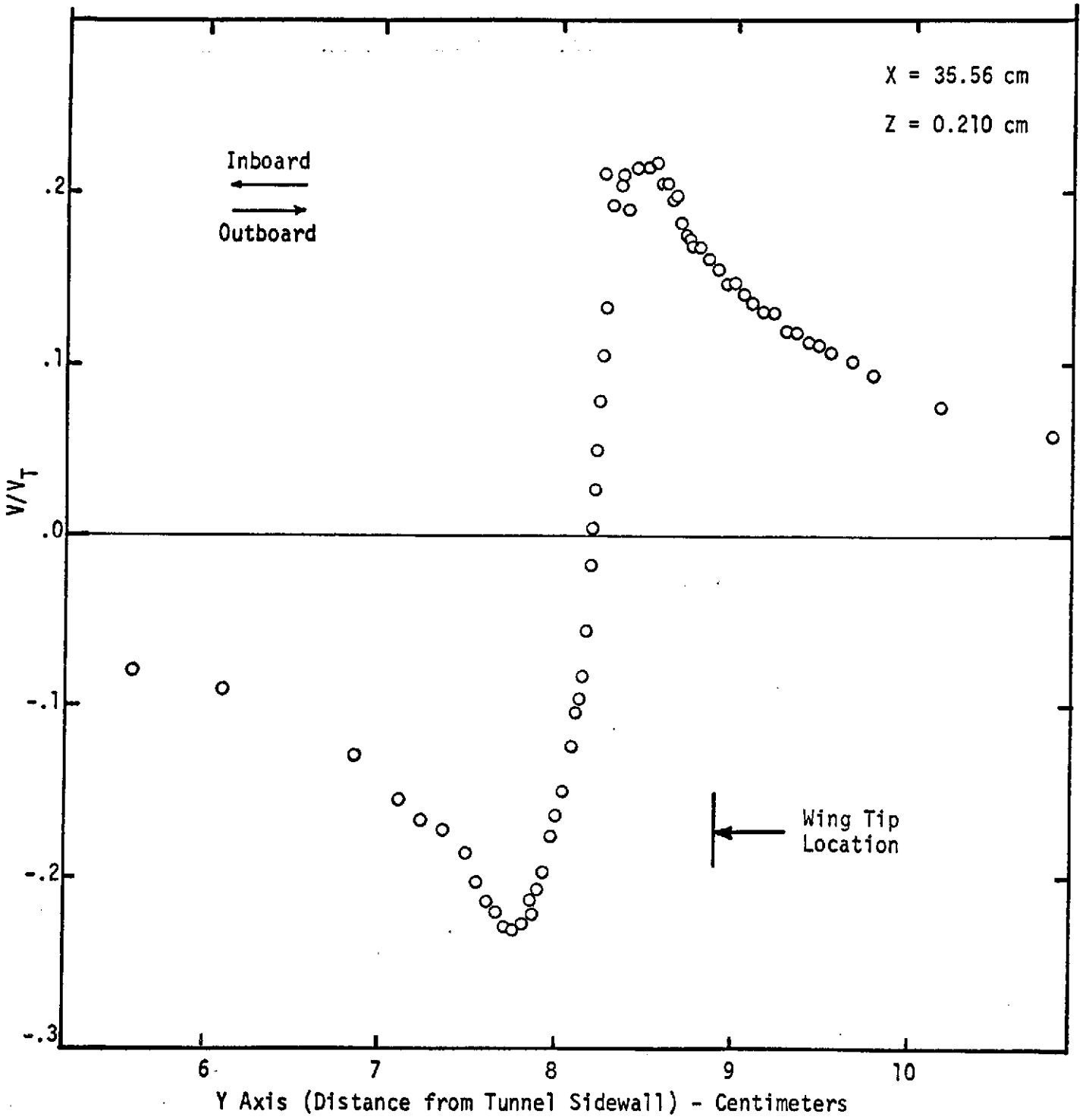

Fig. 26 V Velocity Component Distribution in Wing Tip Vortex

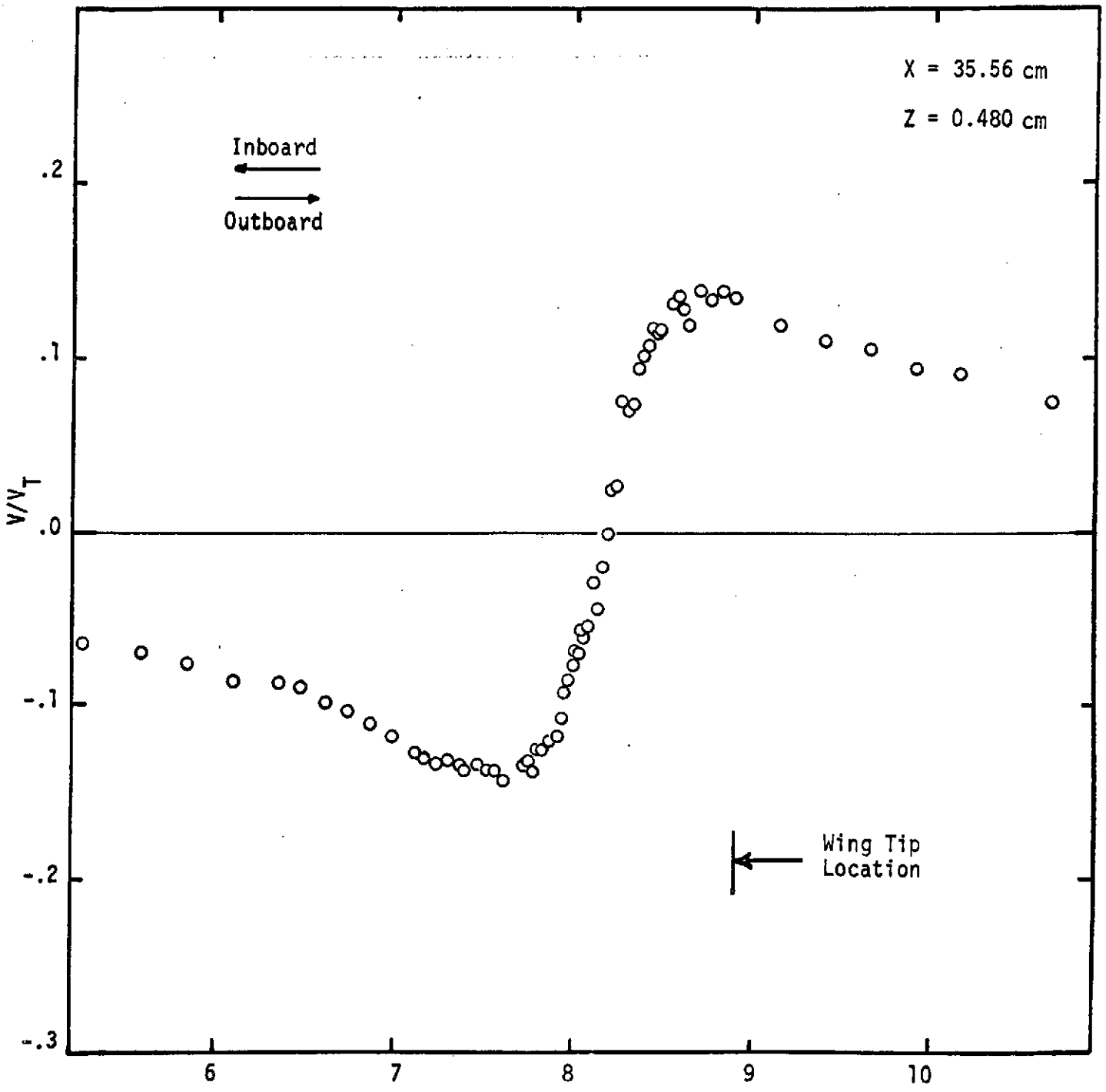

Fig. 27 V Velocity Component Distribution in Wing Tip Vortex

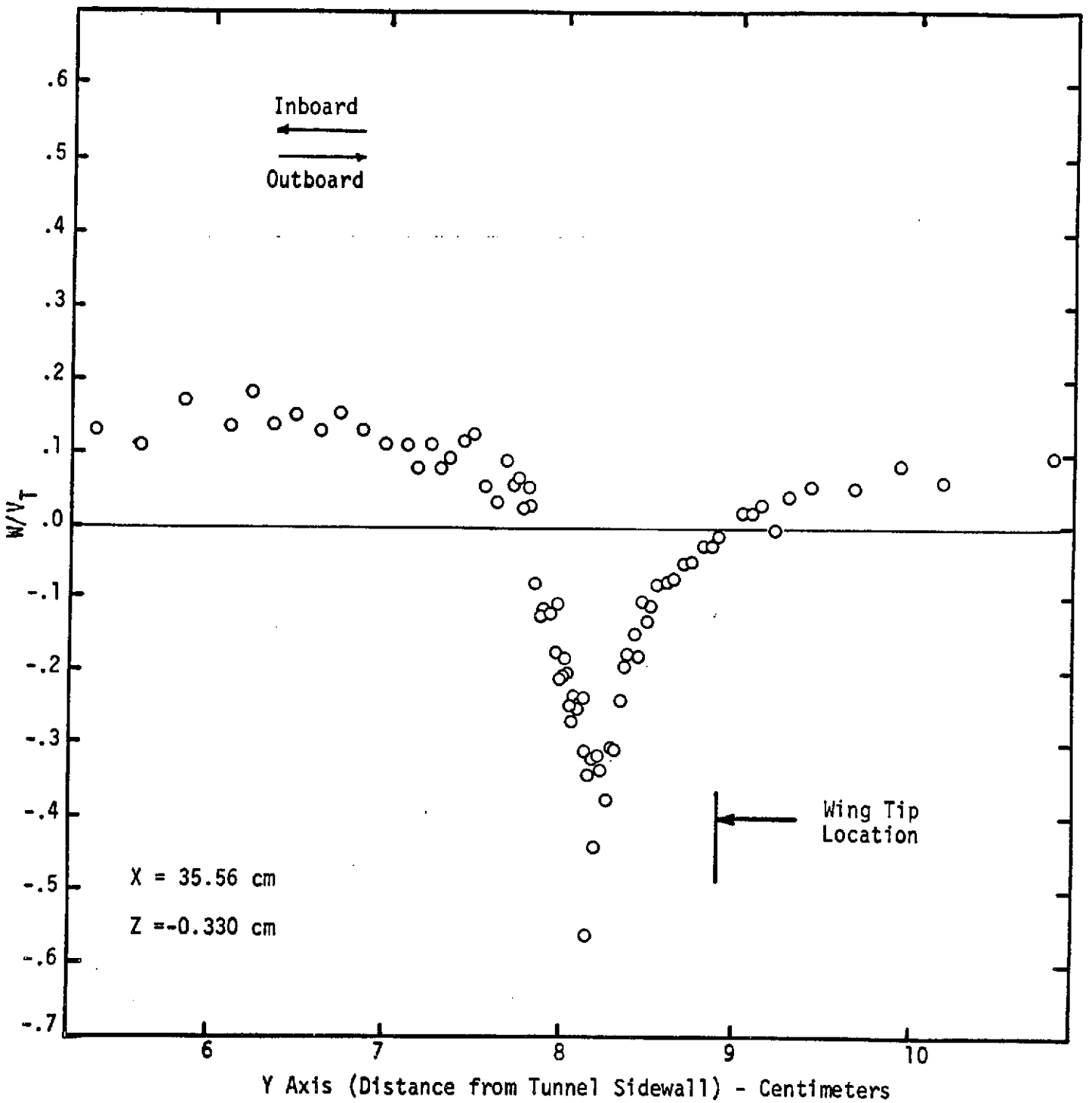

Fig. 28 W Velocity Component Distribution in Wing Tip Vortex

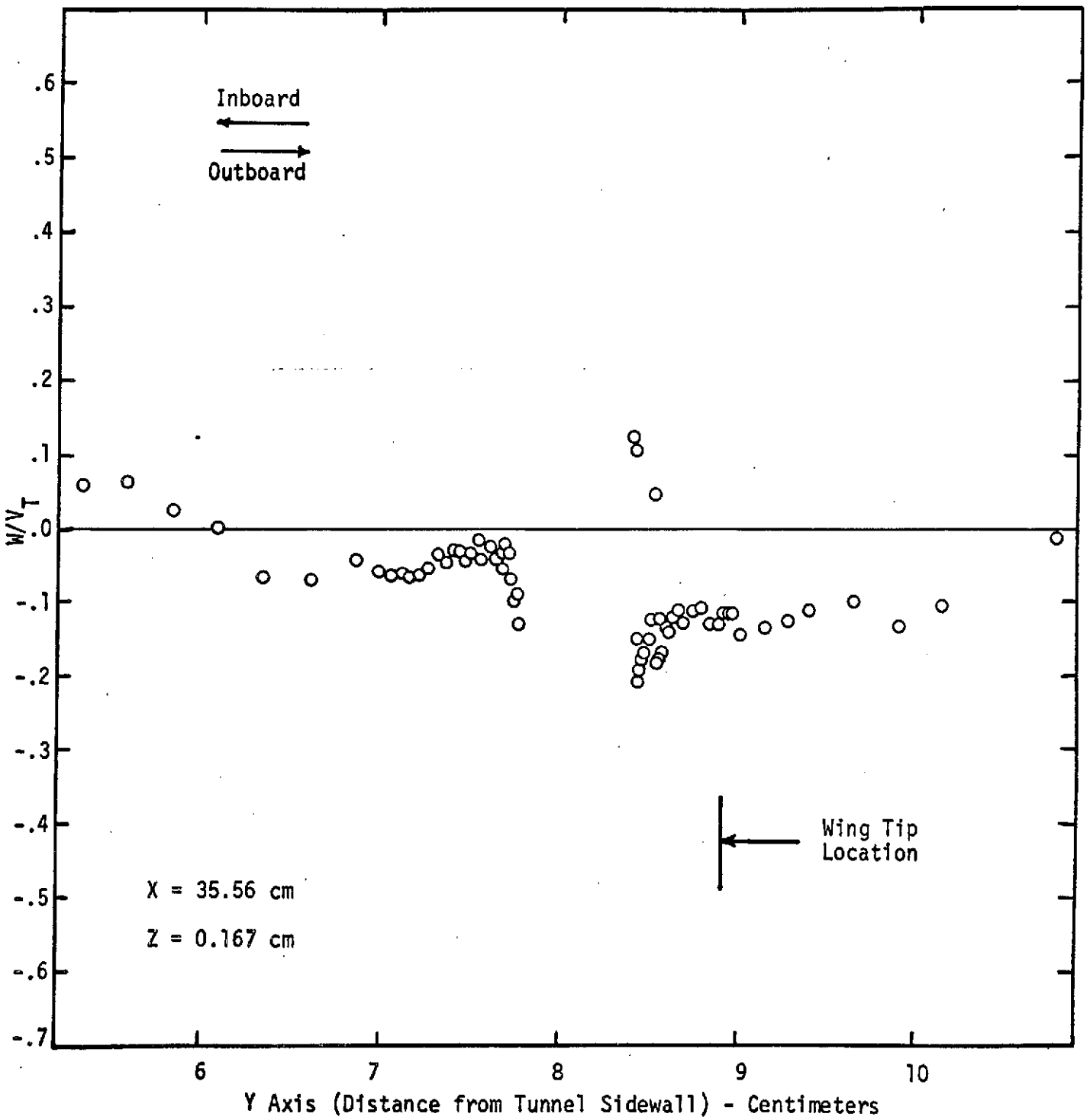

Fig. 29 W Velocity Component Distribution in Wing Tip Vortex

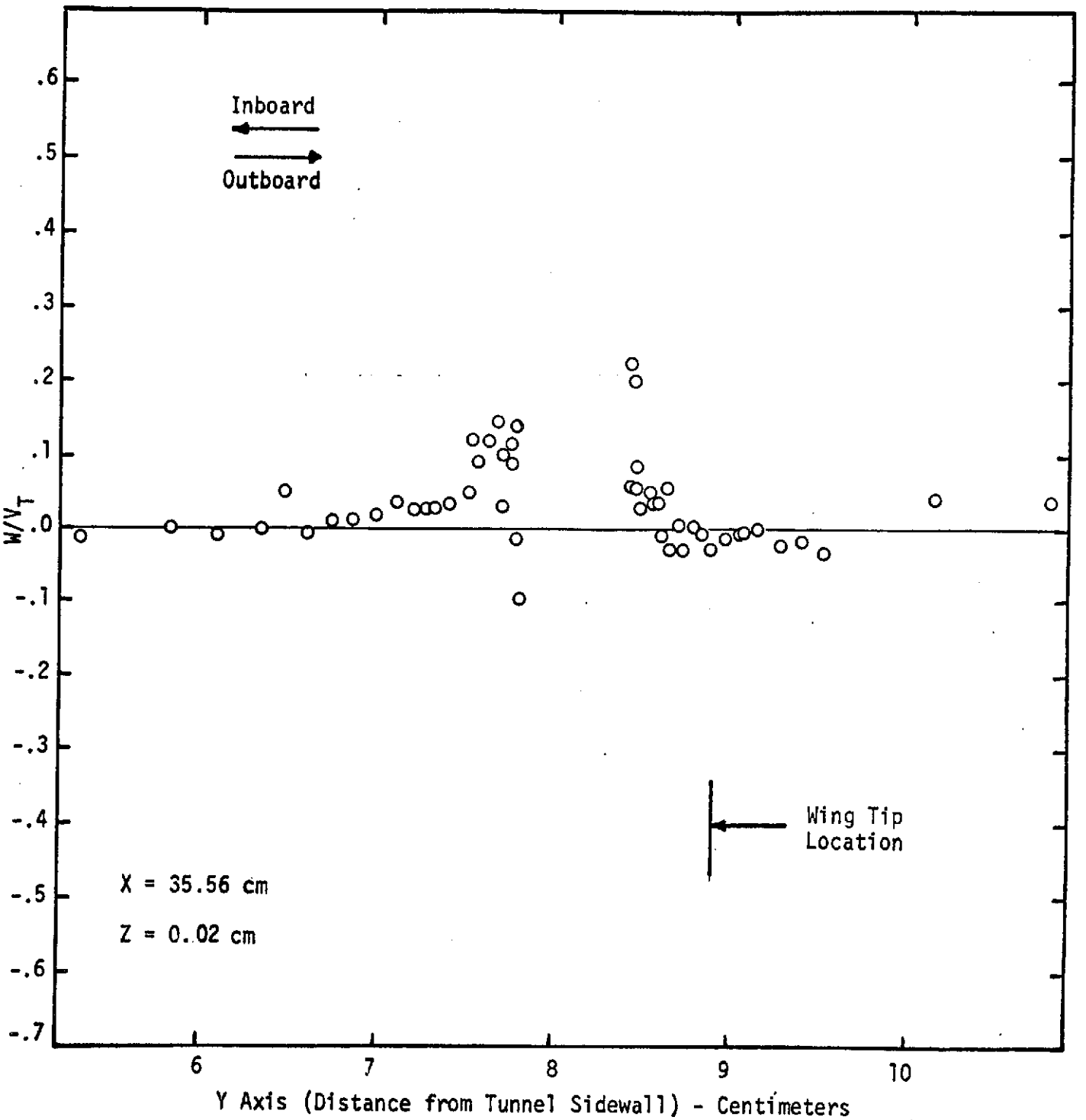

Fig.30 W Velocity Component Distribution in Wing Tip Vortex

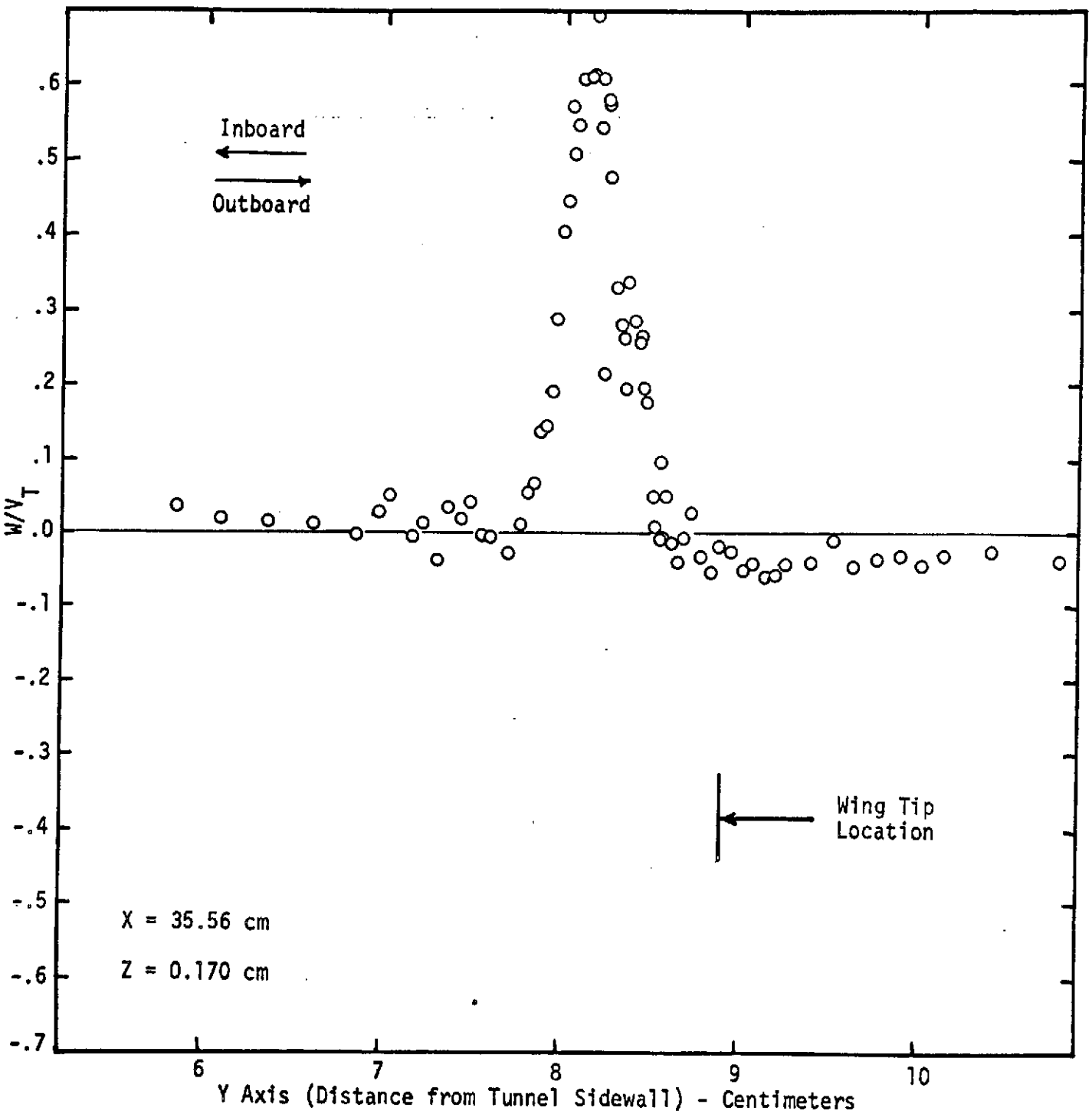

Fig. 31 W Velocity Component Distribution in Wing Tip Vortex

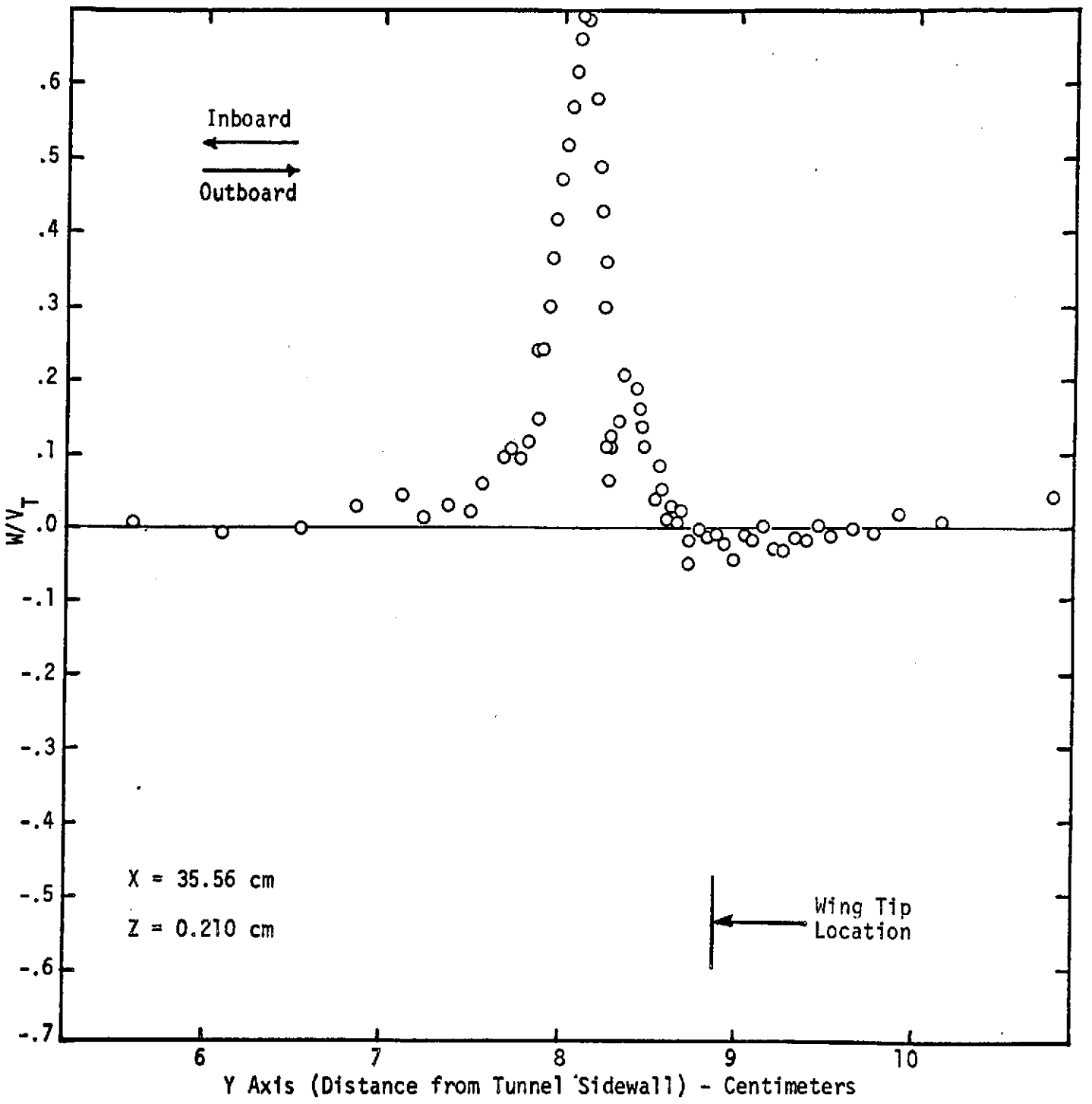

Fig. 32 W Velocity Component Distribution in Wing Tip Vortex

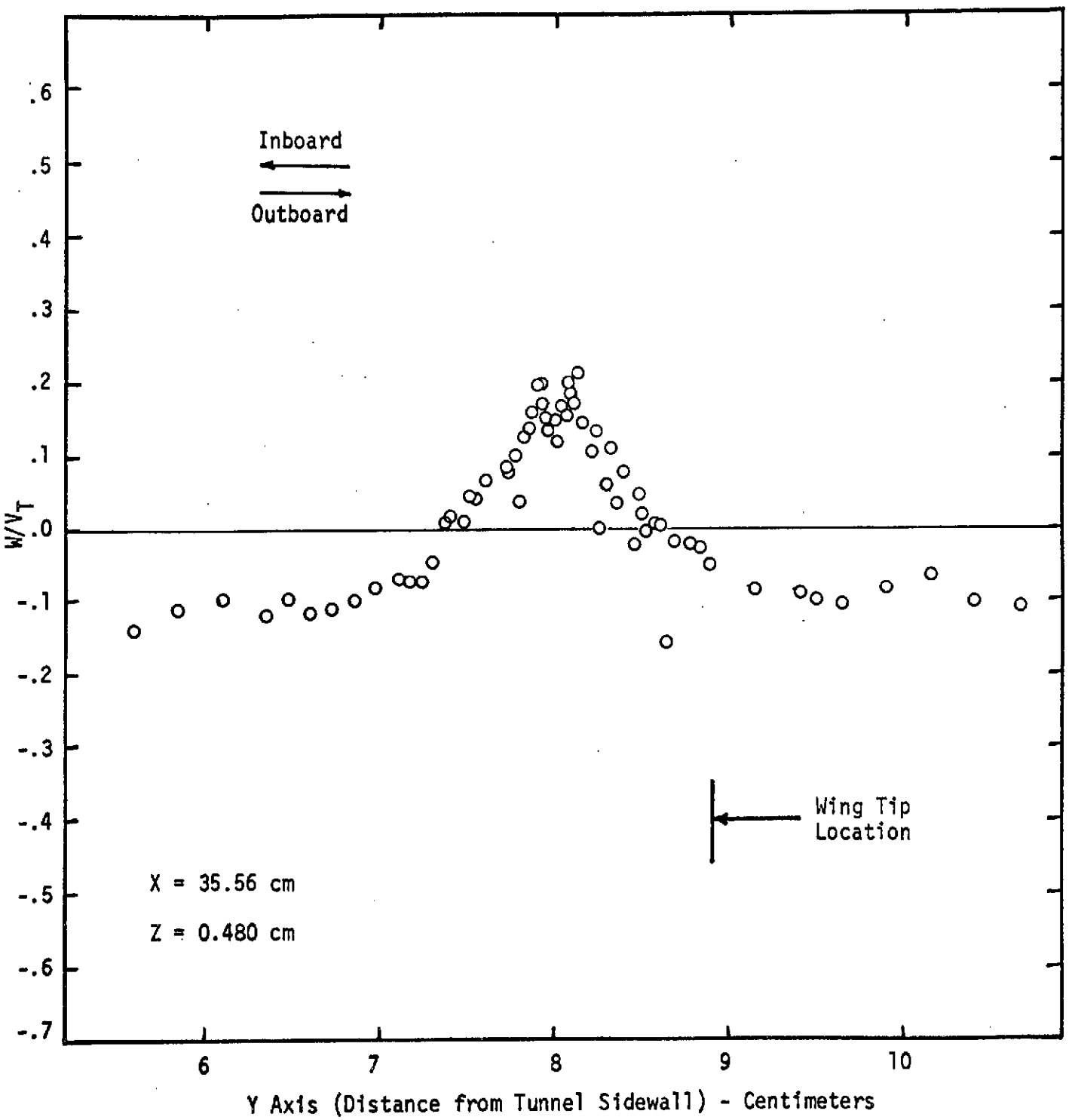

Fig. 33 W Velocity Component Distribution in Wing Tip Vortex

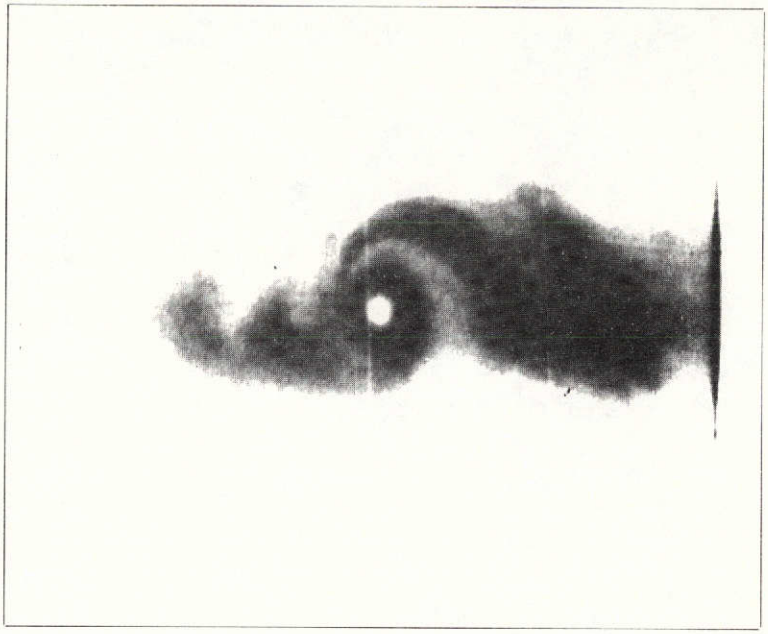

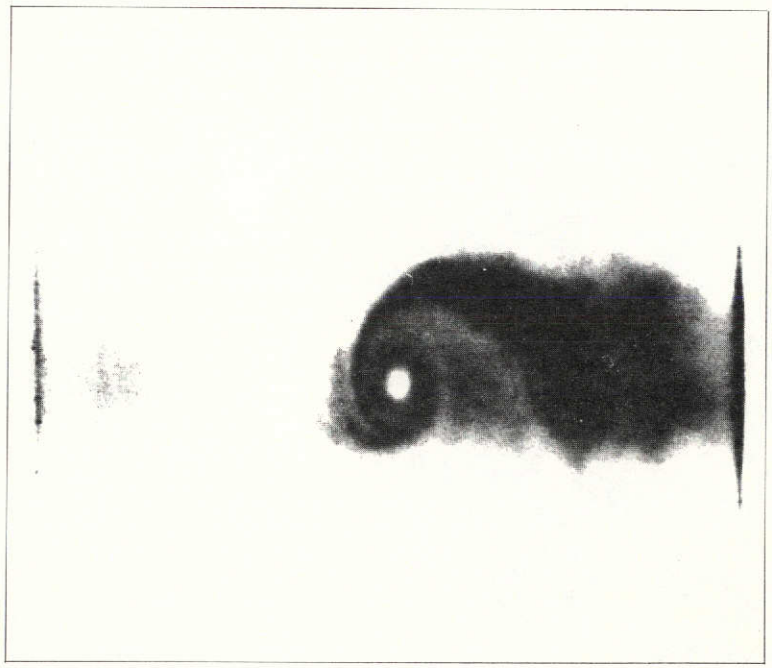

Figure 34 Visual Display of Wing Tip Vortex Pattern in MSFC 7 X 7 Inch Wind Tunnel at 7 Inch Downstream of Wing Trailing Edge.

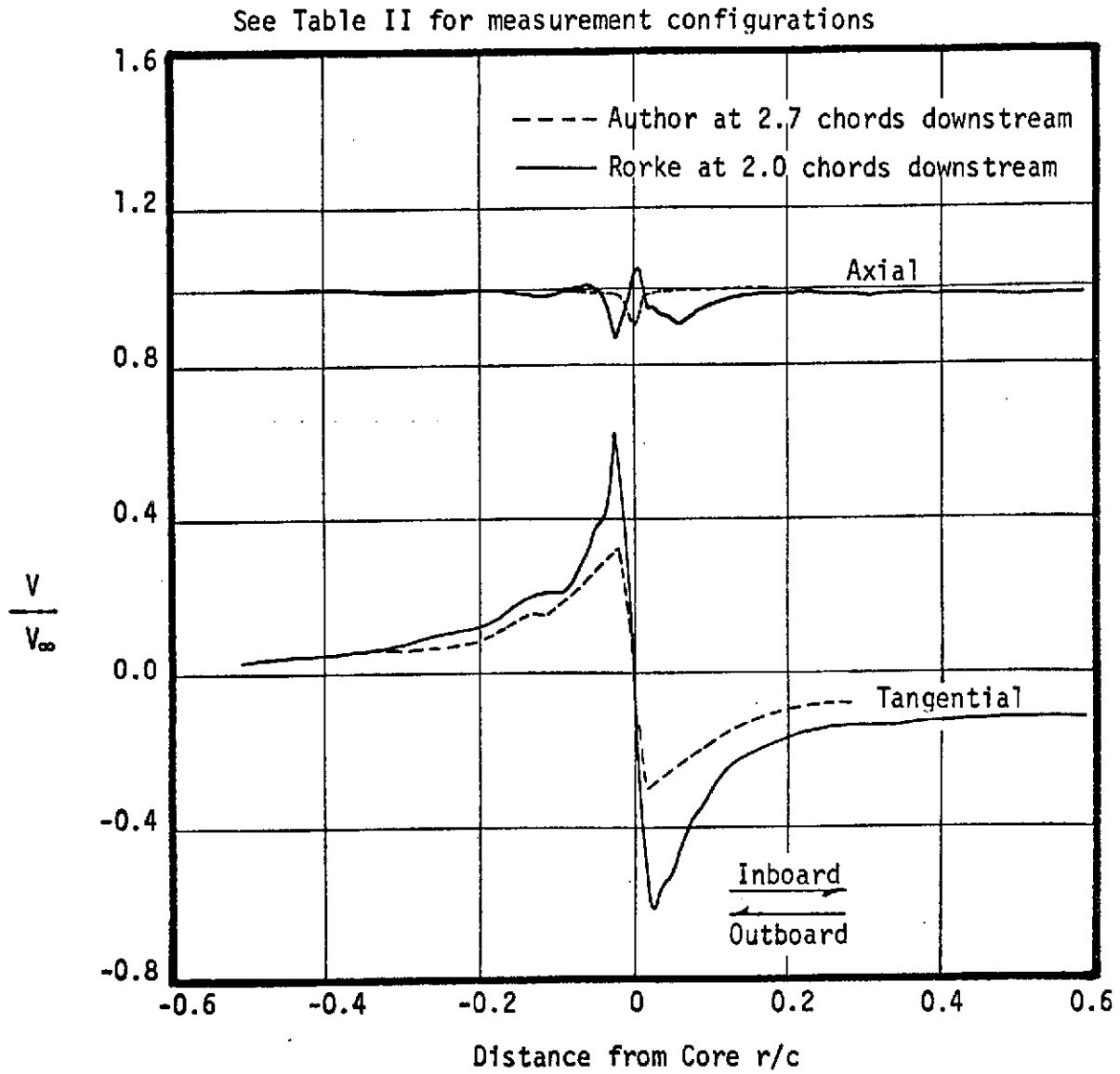

Fig. 35 Comparison of Vortex Velocity Distributions

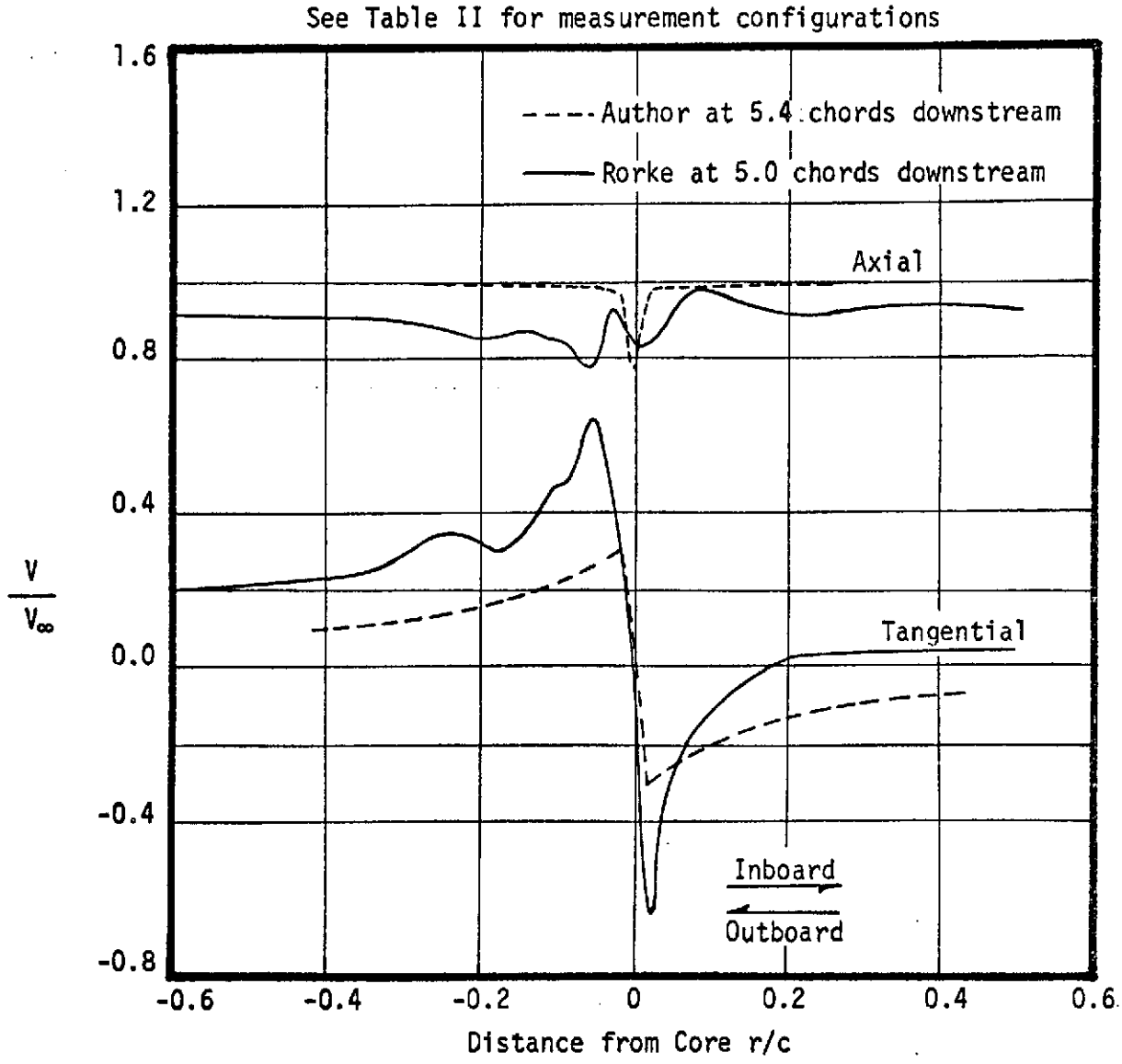

Fig. 36 Comparison of Vortex Velocity Distributions

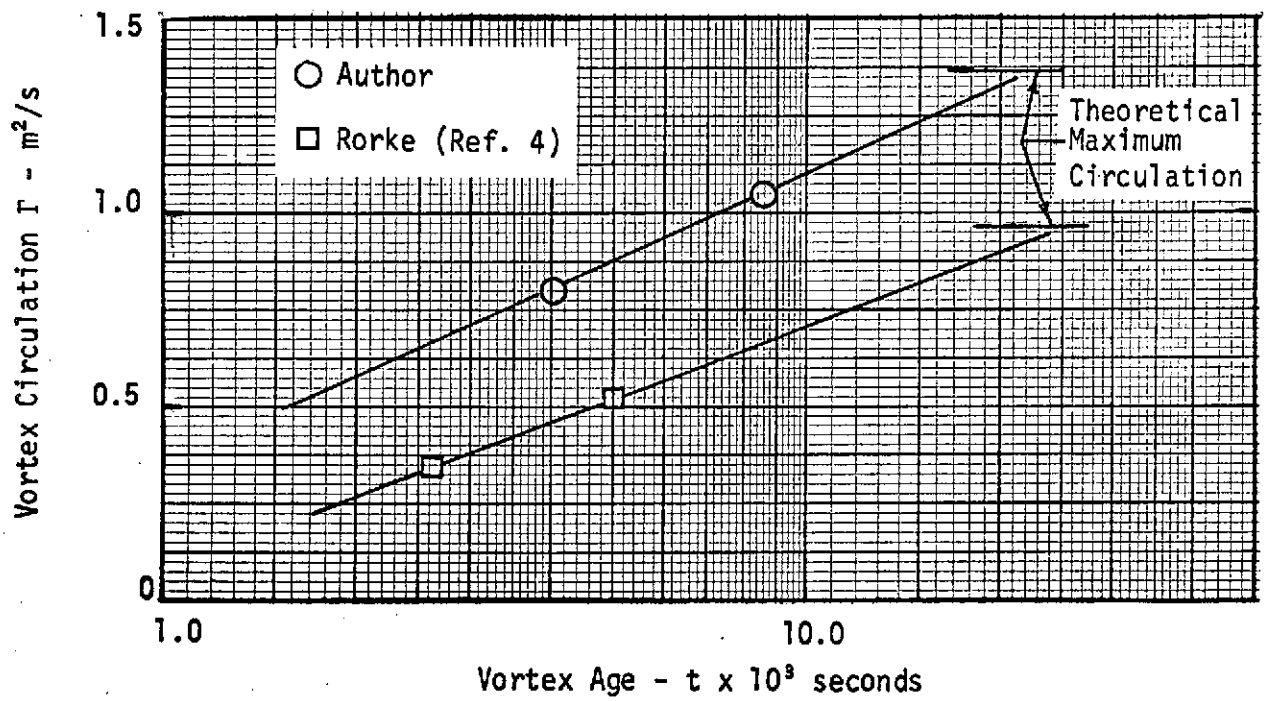

Fig. 37 Comparison of Vortex Circulation as a Function of Vortex Age

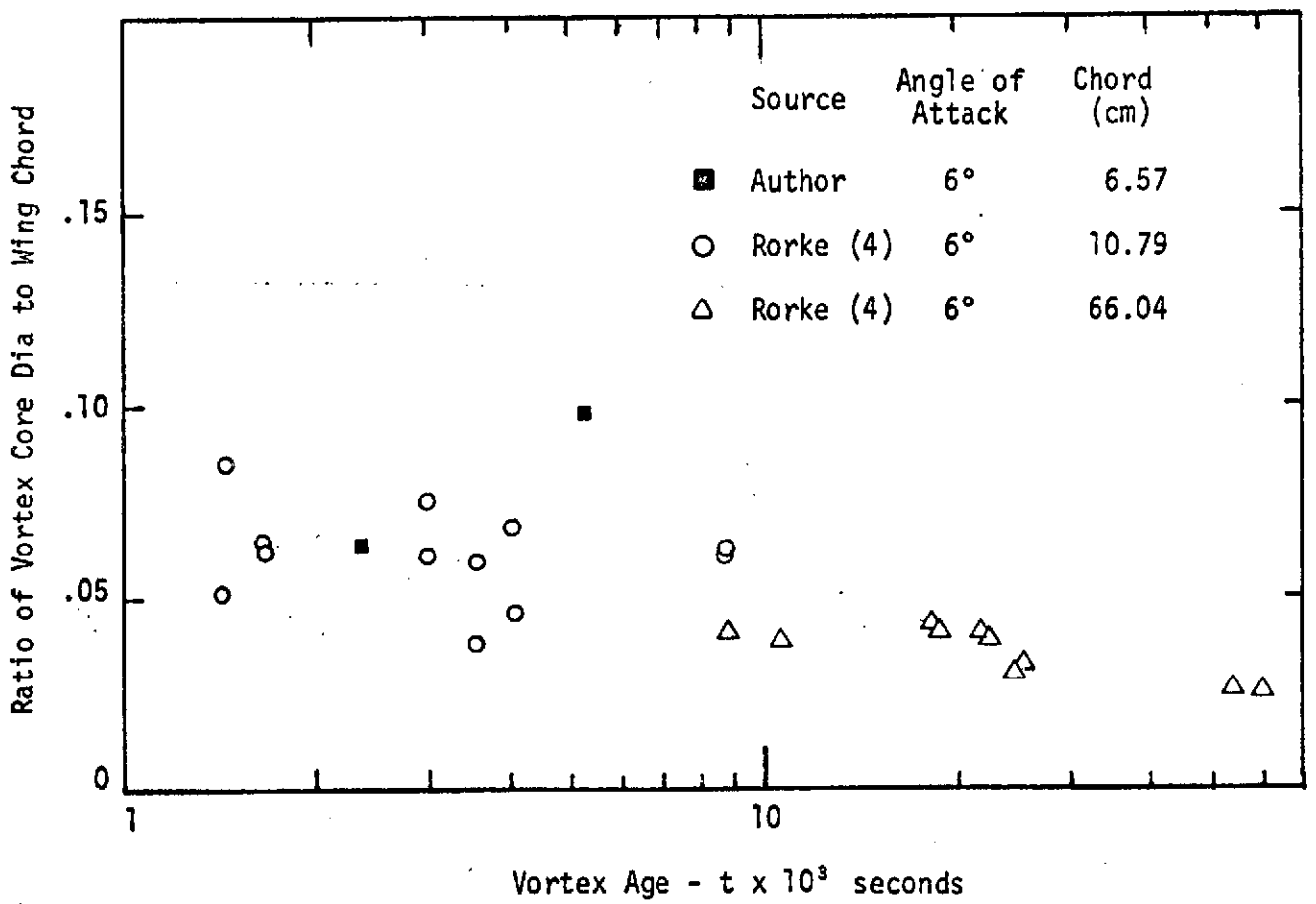

Fig. 38 Comparison of Vortex Core Diameter Variation with Vortex Age.

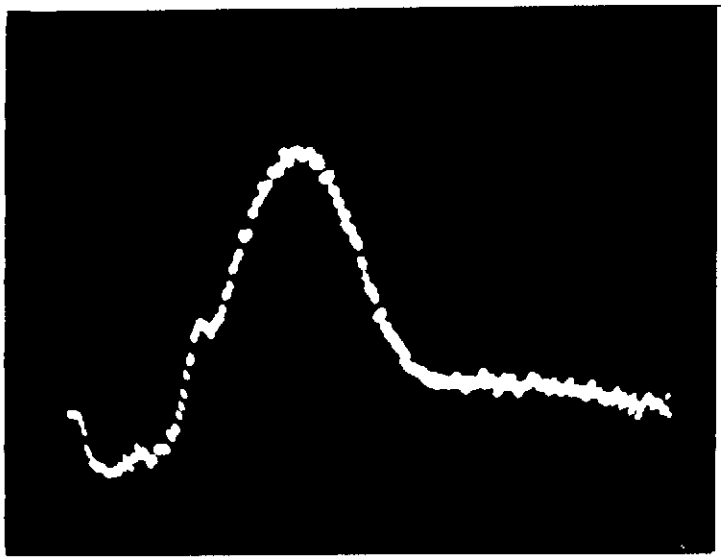

Signal Trace Outside Core Region.

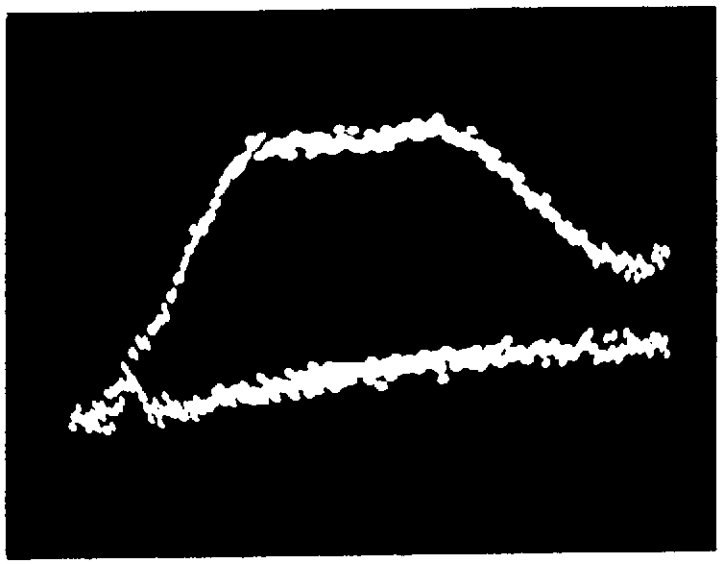

Signal and Noise Trace Close to Core - Note the Broadness.

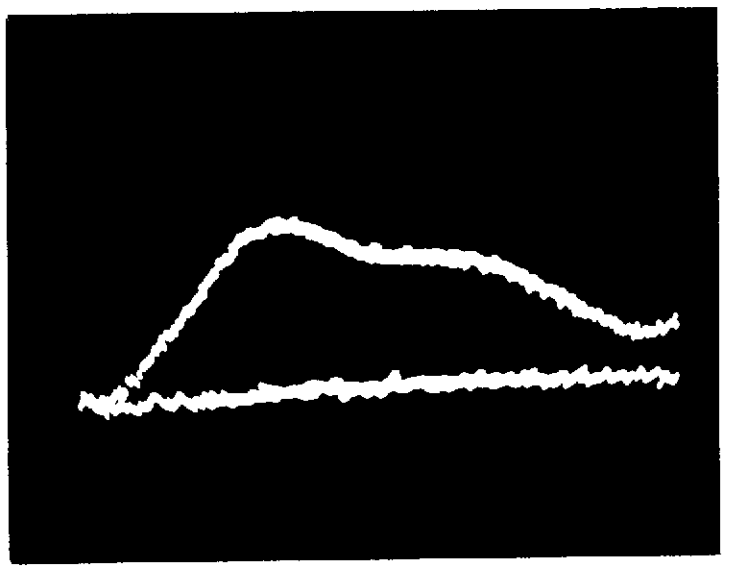

Signal and Noise Trace Slightly Closer to Core - Note Amplitude Reduction and Double Hump Nature of Signal.

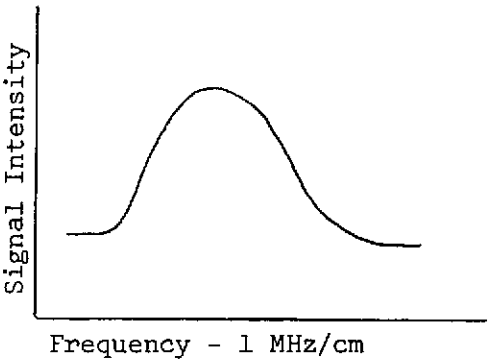

Figure 39 Doppler Frequency Spectrums of F_1 Component Showing Changes at Points Close to the Vortex Core.

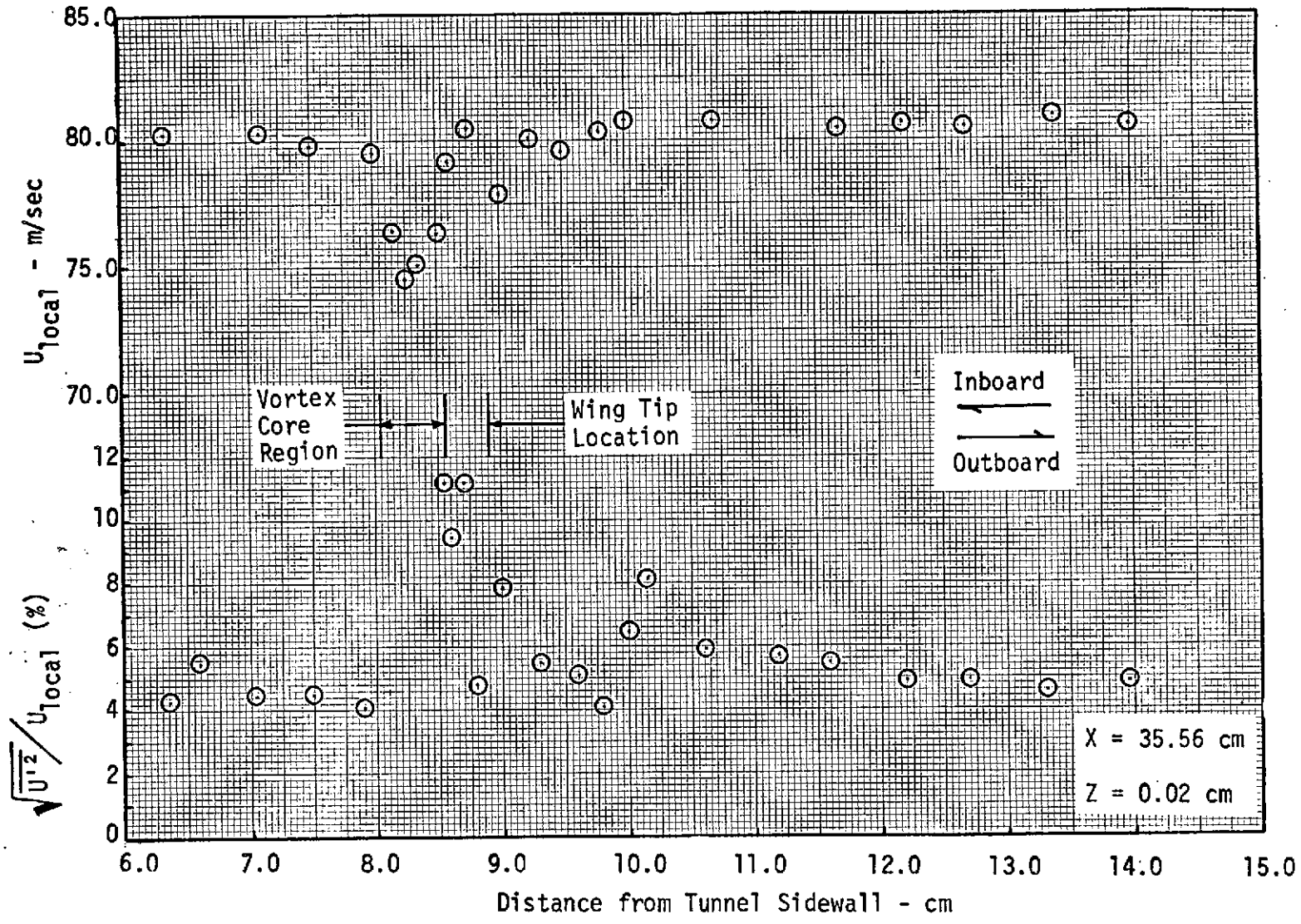

Fig. 40 Axial Mean Velocity and Turbuelnce Measurements with 1-D LDV System.

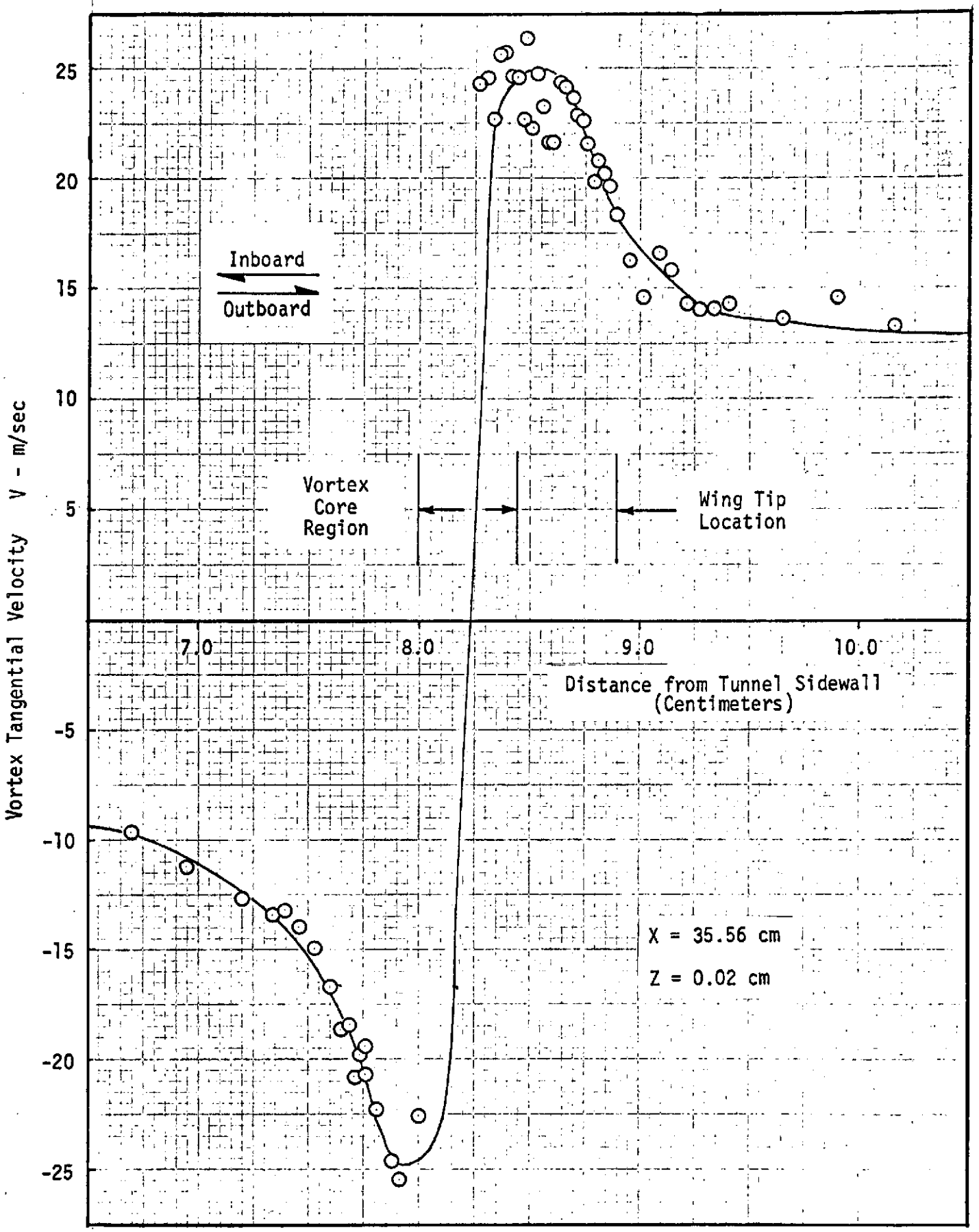

Figure 41 - Vortex Tangential Velocity Distribution Measured with 1-D LDV Instrument

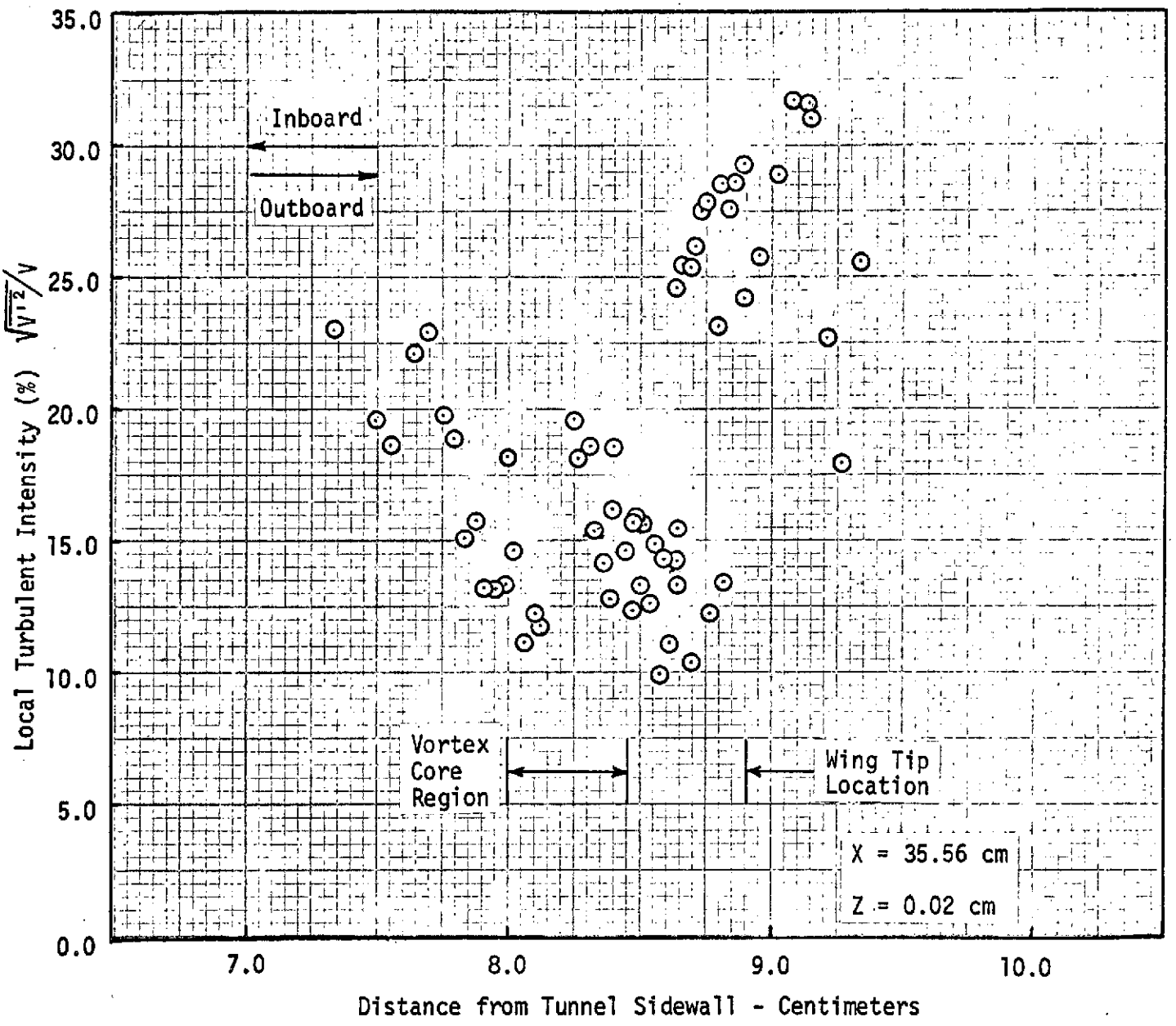

Fig. 42 Tangential Turbulent Intensity Distribution in Vortex Measured with 1-D LDV System